Study on Performance Analysis of Heat Pump Cycle Using Model-based Design

NAKATSU, Hideaki
九州大学大学院総合理工学府総合理工学専攻機械・システム理工学メジャー

https://hdl.handle.net/2324/7178778

出版情報：Kyushu University, 2023, 修士, 修士
バージョン：
権利関係：

Master Thesis

Study on Performance Analysis of Heat Pump Cycle Using Model-based Design

Thermal Energy Conversion Systems Laboratory,
Mechanical and Systems Engineering Major,
Interdisciplinary Graduate School of Engineering Sciences,
Kyushu University

Hideaki Nakatsu

Supervisor(s) Takahiko Miyazaki

Kyaw Thu

Date: 31, January, 2024

Contents

Nomenclature

The main symbols and subscripts used in this paper are as follows

.

Symbols

A	Area	m^2
c_p	Specific heat	kJ/kg
COP	Coefficient of performance	-
E	power	kW
f	Friction factor	-
G	Mass velocity	kg*m/s
h	Enthalpy	kJ/kg
HTC	Heat transfer coefficient	kW/m^2K
k	Thermal conductivity	kW/(m*K)
L	Length	m
$LMTD$	Logarithmic mean temperature difference	K
m	Mass flow rate	kg/s or kg/h
M	Fluid mass	kg
N	Compressor rotation speed	rpm
Nu	Nusselt number	-
P	Pressure	kPa
Pr	Prandl number	-
Q	Heat exchange amount	kW
R	Thermal resistance	K/kW
Re	Reynolds number	-
T	Temperature	℃
u	Internal energy	kJ/kg
$\bar{u}$	Normalized internal energy	-
UA	Overall thermal conductance	kJ/K
W	Work	kW
x	Vapor quality	-
η	efficiency	-
μ	Viscosity	Pa*s

ρ	density	Kg/m^3
v	Volume	m^3
ε	roughness	m
σ	Surface tension	N/m
Φ	Energy flow	kW

Subscripts

adi	Adiabatic
B	Antifreeze
c	cooling
Comp	Compressor
Cond	Condenser
d	Compressor discharge
D	Diameter
Evap	Evaporator
h	Heating
H	Heat sink/source
ideal	Ideal
in	inlet
L	Liquid
min	minimum
max	max
out	outlet
Ref	Refrigerant
s	Compressor suction
sat	saturation
V	Vapor
vol	volmetric
W	Water

1. Introduction

1.1. Research background

With the rapid economic and population growth in recent years, energy consumption also increased significantly. It causes climate change such as global warming and air conditioning and refrigeraton will be more important. For an environmentally friendly and sustainable world, improvement of energy management is also important.

In air conditioners and refrigerators, heat pump system is used and refrigerant is the working fluid in the system. Currently HFCs (hydro-fluoro-carbons) have been widely used as refrigerant. However, the HFCs have high GWP(Global Warming Potential) and should be converted to low GWP refrigerants by Kigali amendment to the Montreal Protocol[1]. The options for alternative refrigerants are natural refrigerants such as CO_2 and ammonia, HFOs(hydro-fluoro-olefin), and the mixture of HFCs and HFOs. The refrigerants have their own characteristics and challenges such as very high pressure, toxic, and low volumetric capacity. So the alternative refrigerants should be used appropriately for each application.

In industries, thermal management by 3R(Reduce, Reuse, Recycle) is important. Reduce is reducing thermal energy by insulation and heat storage technology and Recycle is exchanging heat to other energy such as waste heat power generation. The Reuse is use the waste heat again as heat. According to the survey in Japan, heat under 200℃ accounts for 76% in total waste heat from factories[2],[3]. Heat pump is expected to reuse the low temperature waste heat and improve thermal management.

To expand heat pump technology, optimum refrigerant should be selected according to the running condition and combination with other electric or thermal systems should be considered. This study focuses on developing heat pump that can be applied to wide range with model-based design.

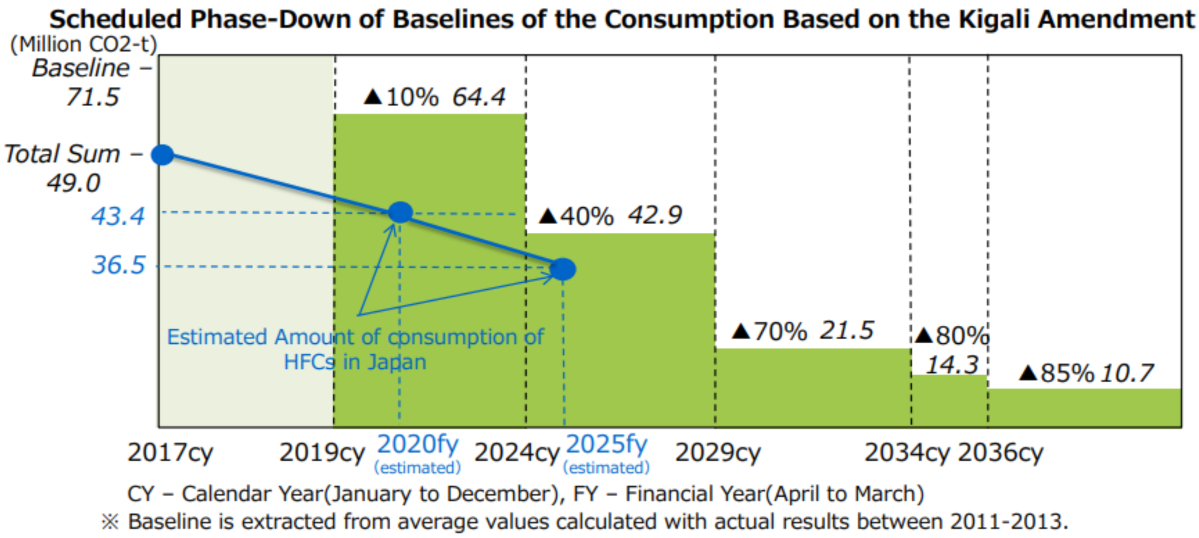

Fig. 1.1 HFC reduction schedule under the Kigali amendment in Japan[1]

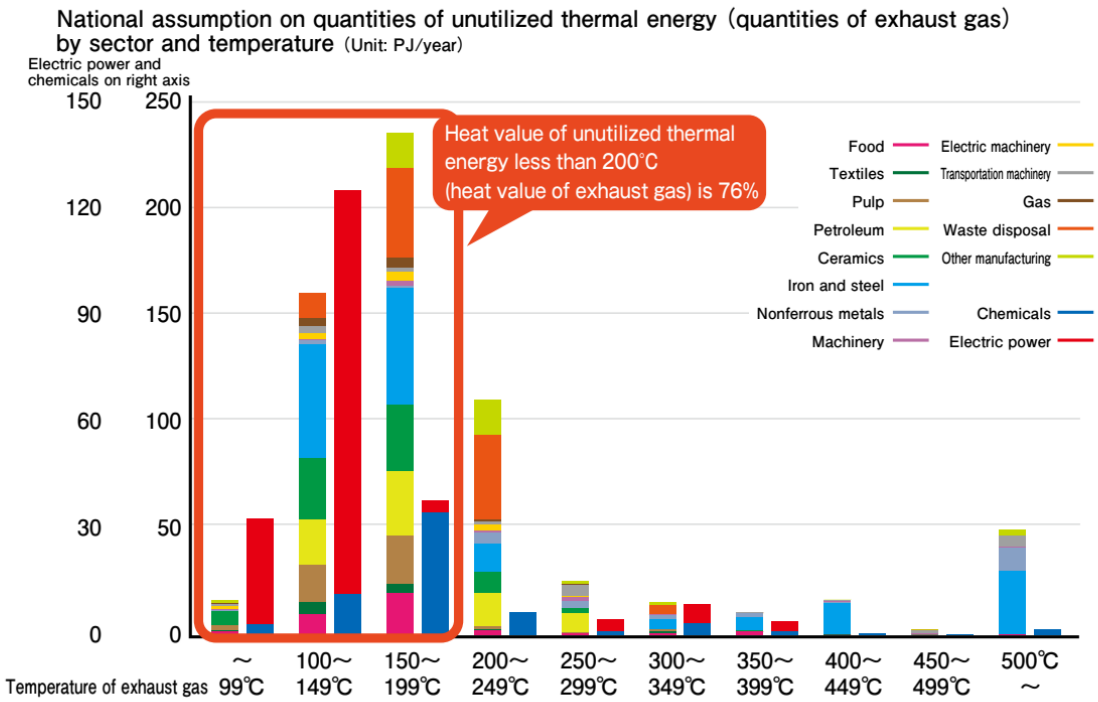

Fig. 1.2 Utilization temperature and exhaust heat temperature of industrial sector heat demand[3]

1.2. Overview and previous research

1.2.1. Heat pump and zeotropic mixture

Basic heat pump consists of compressor, condenser, expansion valve, and evaporator. Fig. 1.3 shows the *P-h* diagram and *T-s* diagram of heat pump cycle using pure refrigerant. 1→2 is compression process in compressor, 2→3 is condensation process in condenser, 3→4 is expansion process in expansion valve to decrease refrigerant pressure, and 4→1 is evaporation process in evaporator. In heating mode, the heat is supplied from refrigerant in condensation process(2→3) and in cooling mode, the heat is deprived in evaporation process(4→1).

Fig. 1.4 (a), (b) show the *T-s* diagram of the reversed Carnot cycle (1-2-3-4) in pure refrigerant and Lorenz cycle (1'-2'-3'-4'), the cycle when the refrigerant is zeotropic mixture. In condensation and evaporation process, temperature of zeotropic mixture changes since the composition of saturated vapor and saturated liquid is different. This is called saturation temperature glide or simply temperature glide. In ideal case, the temperature difference between refrigerant and heat sink/source fluid can decrease in condensation and evaporation process and contribute to improving the efficiency (reduction of green area). But in actual case, it is known that the resistance happens during condensation and evaporation process. Fig. 1.4 shows the distribution of the fraction of high boiling point component and temperature in condensation. During condensation, high boiling point component is dominant in liquid phase and low boiling point is dominant in vapor phase. That causes the gradient of temperature and decreases the effective temperature difference between refrigerant and wall. That contributes to decreasing heat transfer coefficient. This is called mass transfer resistance. Therefore, the condensation and evaporation pressure and temperature are higher than ideal case as shown in Fig. 1.4(b) (increase orange area power input). If temperature glide work effectively than influence of mass transfer resistance, cycle performance improves and will be higher than that of pure refrigerant.

Fukuda rt al[4] et al conducted experimental research on cycle performance and irreversible losses in the cycle in Cooling mode and Heating mode when zeotropic mixture of R744/R32/R1234yf and R744/R32/R1234ze(E) that GWP is around 300 is drop in to the cycle. The cycle characteristics of binary mixture of R32/R1234yf and ternary mixture of R32/R1234yf/R744 that GWP is 150 are conducted in Cooling and Heating mode byTakezato[5] and in refrigeration mode by Kawagita[6]

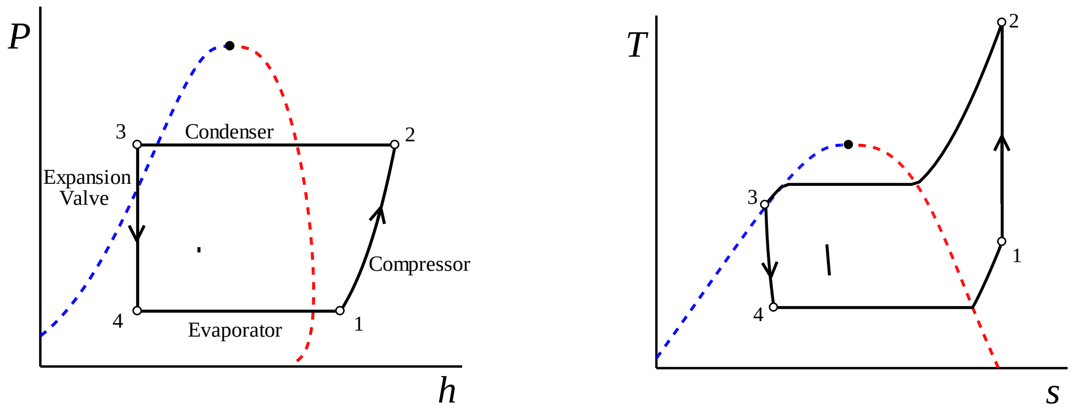

(a) *P-h* diagram (b) *T-s* diagram

Fig. 1.3 Schematic diagram of heat pump cycle

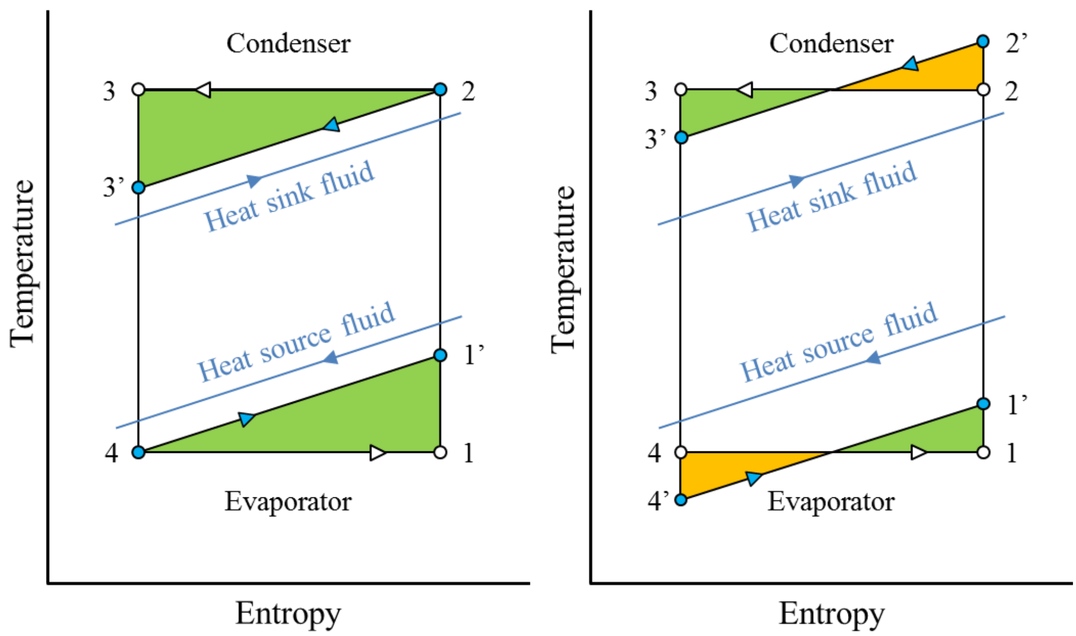

(a) (b)

Fig. 1.4 Reversed Carnot cycle and Lorenz cycle

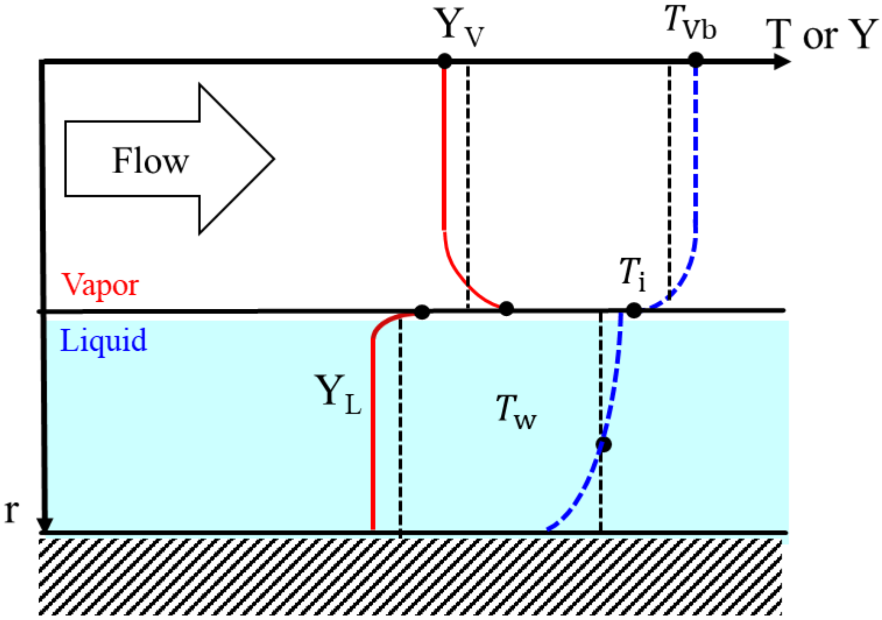

Fig. 1.5 Distribution of mass fraction and temperature

1.2.2. Model-based design and Simscape

Model-based design is a simulation method that connect the model blocks and enable to construct complicated model visually and easily and contributes to reducing time for developing the simulation model.

The Simscape is one of the dynamic simulation tool in MATLAB-Simlink and enable to make the physical system easily and visually in Simlink. The Simscape model block includes electricity, thermal, fluid, robotics, multibody, control system, and so on. The Simlink model defines the flow of data from one block to another and uses directional signal connections. The Simscape model uses physical connections and enable to communicate bidirectionally between components with differential algebraic equations (DAEs).

As previous research, Saito et al developed general purpose heat pump simulator "Energy flow + M"[7]. In MATLAB Simscape environment, Singh et al developed dynamic simulation model for house heating using zeotropic mixture R407C[8]. Ko et al simulated CO_2 refrigeration system and predicted the performance of actual system within ±7% error[9].

1.3. Objectives and structures

Heat pump is important technology for both of air conditioning and refrigeration, and improvement of thermal management in industries. At the same time, the current refrigerant should be converted to environmentally friendly one to decrease the impact to the environment by refrigerant. It takes time and cost to introduce heat pump with the optimum alternative refrigerants to various fields. However, Simscape can simulate combining with other thermal, electrical, and mechanical systems and enable to accelerate analysis and evaluation of introducing heat pump to various field from household scale to industrial scale. In this study, the versatile heat pump cycle model that can be applied to various systems is developed with Simscape.

This thesis consists of 5 chapters. Chapter 1 is the background about current and alternative refrigerants, and review of experimental research of alternative refrigerants and previous study of het pump modeling with model-based design.

Chapter 2 summarize the experimental apparatus, the experimental methods, the experimental conditions.

Chapter 3 describes the analysis of refrigerants heat transfer in the heat exchanger and the comparison of heat transfer coefficient correlation.

Chapter 4 describes the structure of the heat pump model on Simscape, comparative evaluation of experiment and simulation, and challenges of modeling.

Chapter 5 lists the conclusion of this study.

2. Experimental method

2.1. Experimental apparatus

Figure 2.1 shows a schematic diagram of the experimental apparatus. The experimental apparatus is a vapor compression heat pump and consists of a refrigerant loop and heat source/sink water loop. The refrigerant loop consists of a scroll compressor, oil separator, condenser, electronic expansion valve, and evaporator, shown in red and blue in the figure. The heat source/sink loop consists of a constant-temperature bath, a heat exchanger, and a pump, shown as black lines in the figure. The thermocouple and pressure sensor are set at inlet/outlet of the compressor, condenser, expansion valve, and evaporator. A mass flow meter is installed between the condenser and the expansion valve to measure the refrigerant flow rate, and there is a sampling port to measure the circulating composition of the refrigerant mixture. In both of heat source and heat sink water, the water discharged from the thermostatic bath by the pump returns to the constant-temperature bath after heat exchange with the refrigerant in the heat exchanger.

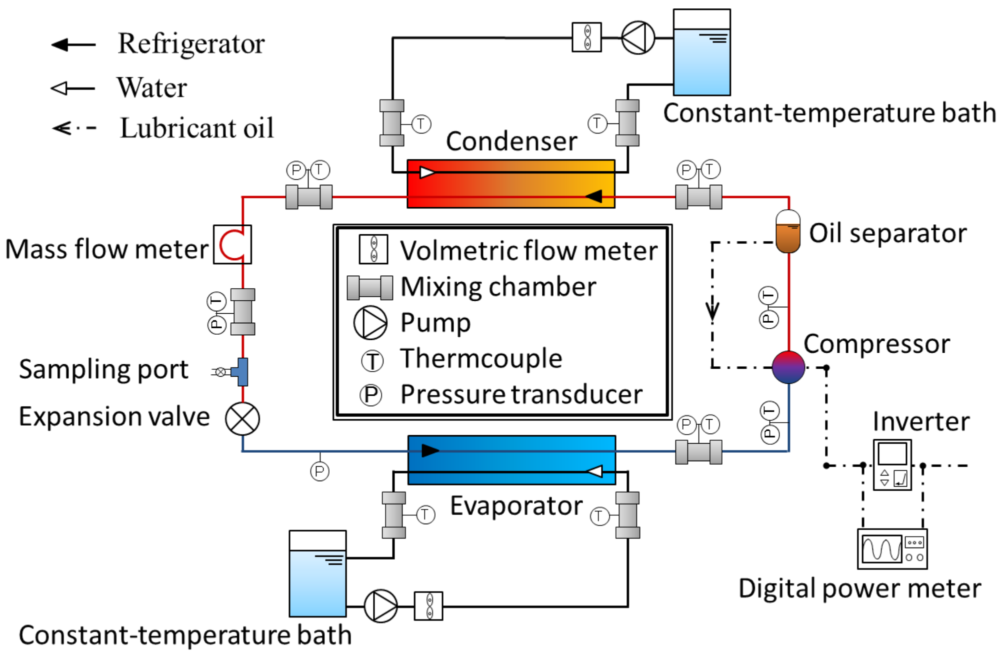

Fig. 2.1 Schematic diagram of the experimental apparatus

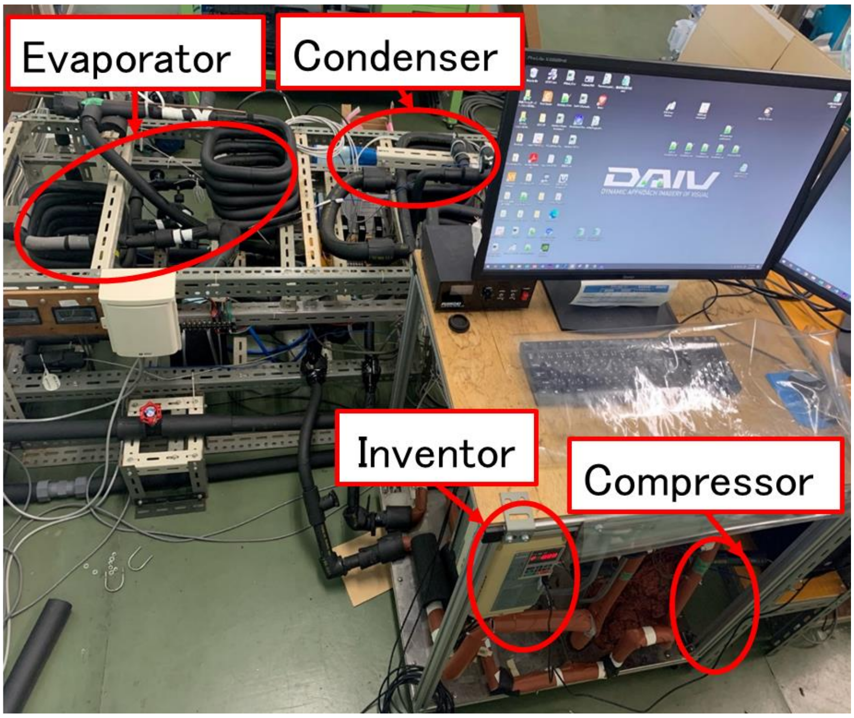

Fig. 2.2 Experimental apparatus

Table 2.1 Specification of heat exchanger

		Outer diameter[mm]	Inner diameter[mm]	Length [mm]	Type
Condenser and Evaporator	Outer tube	15.88	13.88	7200	Smooth
	Inner tube	9.52	7.52	7200	Microfin

Table 2.2 Specification of micro-fin tube

	Number of fin [-]	Fin height H_f [mm]	Spiral angle η [°]	Helix angle α_f [°]
Microfin tube	65	0.15	25	85
	Weight per length [g/m]	W_g [mm]	t_w [mm]	Inner surface area [mm^2/cm]
	128	0.075	7200	369

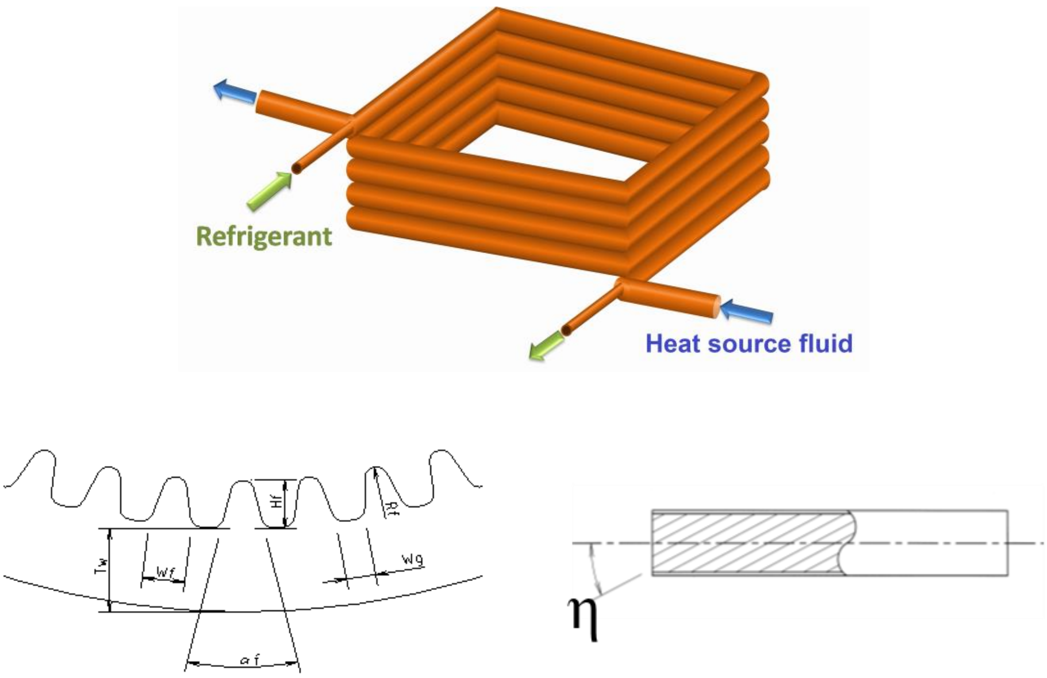

Fig. 2.3 Schematic diagram of heat exchanger

Table 2.3 Specification of compressor

Type	Hermetically sealed electric compressor
Type of compression mechanism	Scroll
Range of operatable rotation speed [rpm]	1500~6000
Upper discharge temperature [°C]	120
Oil	Polyol ester viscosity grade VG68
Cylinder volume [cm^3]	11

Table 2.4 Specification of expansion valve

Type	4-phase stepping motor
Way of excitation	Unipolar drive, 1-2 phase excitation
excitation velocity [pps]	83.33
Upper pressure[MPa]	4.15
Upper pressure ratio [MPa]	3.63

2.2. Methods of measurement and data collection

2.2.1. Pressure measurement

Table 2.5 shows the type of pressure sensor, measuring range, accuracy, and measuring points. The refrigerant pressure before the condenser inlet mixing chamber is measured by an absolute pressure transducer (PHS-50KA, Kyowa Dengyo Co., Ltd.) with a full scale of 5 MPa, and the refrigerant pressure after the condenser inlet mixing chamber, at the compressor outlet, condenser outlet and electronic expansion valve inlet is measured by an absolute pressure sensor (PHS-B-5MP, Co. Kyowa Dengyo Co. The refrigerant pressure before the mixing chamber at the evaporator outlet is measured by an absolute pressure sensor (PHS-20KA, Kyowa Dengyo Co., Ltd.) with a full scale of 2 MPa, and the refrigerant pressure at the evaporator inlet, after the mixing chamber at the evaporator outlet and at the compressor inlet is measured by an absolute pressure senosor (PHS-B-2MP, Kyowa Dengyo Co., Ltd.) with a full scale of 2 MPa. Ltd. The heat source fluid pressures at the condenser inlet and evaporator outlet on the heat source fluid loop side are measured by a full-scale 500 kPa absolute pressure sensor (PSE564, SMC Corporation).

Table 2.5 Pressure measurement

Type of sensor	Measurement range	Accuracy*	Measurement point
Absolute pressure sensor	~5MPa abs	±0.14%RO	Condenser inlet mixing chamber inlet
		±0.17%RO	Condenser inlet mixing chamber outlet
		±0.17%RO	Condenser outlet mixing chamber inlet
		±0.18%RO	Condenser outlet mixing chamber outlet
		±0.18%RO	Compressor outlet
	~2MPa abs	±0.18%RO	Evaporator inlet
		±0.19%RO	Evaporator outlet mixing chamber inlet
		±0.17%RO	Evaporator outlet mixing chamber outlet
		±0.17%RO	Compressor inlet
	~500kPa abs	±0.5%F.S.	Condenser heat sink fluid Inlet/outlet
			Evaporator heat sink fluid Inlet/outlet

2.2.2. Temperature measurement

Table 2.6 lists the type of the thermocouple, measurement range, accuracy, and measurement points. The refrigerant temperature is measured using a sheath of 1.0 mm K-type inserted in the mixing chamber and port in the refrigerant pipe. The temperature of the heat sink/source fluid is measured by sheath diameter 1.0 mm K-type and T-type thermocouples inserted into the mixing chamber at the inlet/outlet of the heat exchanger. The refrigerant temperature at evaporator inlet is calculated by assuming the expansion process is isenthalpy change.

Table 2.6 Temperature measurement

Type of sensor	Range	Accuracy	Measurement point	
Sheathed K-type thermocouple (1.0mm OD)	-15~80°C	±0.05K	Refrigerant	Compressor inlet
				Condenser inlet
				Expansion valve inlet
				Evaporator inlet
Sheathed T-type thermocouple (1.0mm OD)			Heat sink/ source	Condenser inlet/outlet
				Evaporator inlet/outlet
			Environment temperature	

2.2.3. Flow rate measurement

Table 2.7 shows the flowmeter type, measurement range, accuracy, and measurement locations. Refrigerant flow is measured by a Coriolis flowmeter (D025S-SS-200, OVAL Corporation) with a full scale of 220 kg/h. The heat source fluid flow rate is measured by a gear-type volumetric flowmeter (LGV45A30-G03A, OVAL Corporation) with a full scale of 330 L/h. The heat source antifreeze flow rate is measured by an electromagnetic flow meter (EGM1050C, Tokyo Keiso Co., Ltd.) with a full scale of 350 L/h. The heat source fluid flow is controlled by an electric actuator +(TA-MC161/24, IMI Hydronics).

Table 2.7 Flow rate measurement

Sensor type	Range	Accuracy	Measurement point
Coriolis flowmeter	8.1~81kg/h	±0.21%RD	Expansion valve inlet
Volumetric Flow Meter	~370L/h	±0.5%RD	Condenser・Evaporator inlet/outlet
Electromagnetic flowmeter	~350L/h	±0.19%RD	Evaporator inlet/outlet

2.2.5. Circulation mass fraction measurement

In this study, the refrigerant circulation composition was measured for evaluation experiments in non-azeotropic mixed refrigerants. For non-azeotropic mixed refrigerants, the composition of the refrigerant bottle filling and the circulating composition of the refrigerant flowing through the heat pump cycle do not necessarily match. Therefore, it is necessary to collect and analyze the circulating refrigerant to determine its composition in the experimental apparatus.

The circulation composition of refrigerant mixture is measured. For zeotropic refrigerant mixture, the composition of the refrigerant in the bottle and the circulating composition of the refrigerant flowing through the heat pump cycle do not necessarily match. Therefore, it is necessary to collect and analyze the circulating refrigerant to determine the circulating composition in the experimental apparatus.

Figure 2.4 shows a schematic diagram of the gas chromatograph and peripheral equipment to measure the circulating composition of the refrigerant mixture. The sample refrigerant is a small amount of subcooled liquid refrigerant collected from the sampling port before the expansion valve, expanded into a sampling vessel, and completely evaporated. The collected sample gas is analyzed by gas chromatography. The vapor in the sampling vessel is sampled in small quantities (about 3 mL) by an auto gas sampler and then sent to the gas chromatograph together with helium (He) as a carrier gas. Each component of the refrigerant mixture is separated in a column in the gas chromatograph, and the chromatocorder outputs the area of each component via a detector. The area ratio of each component is then converted to a mass fraction using an area modification factor prepared in advance to obtain the circulating composition.

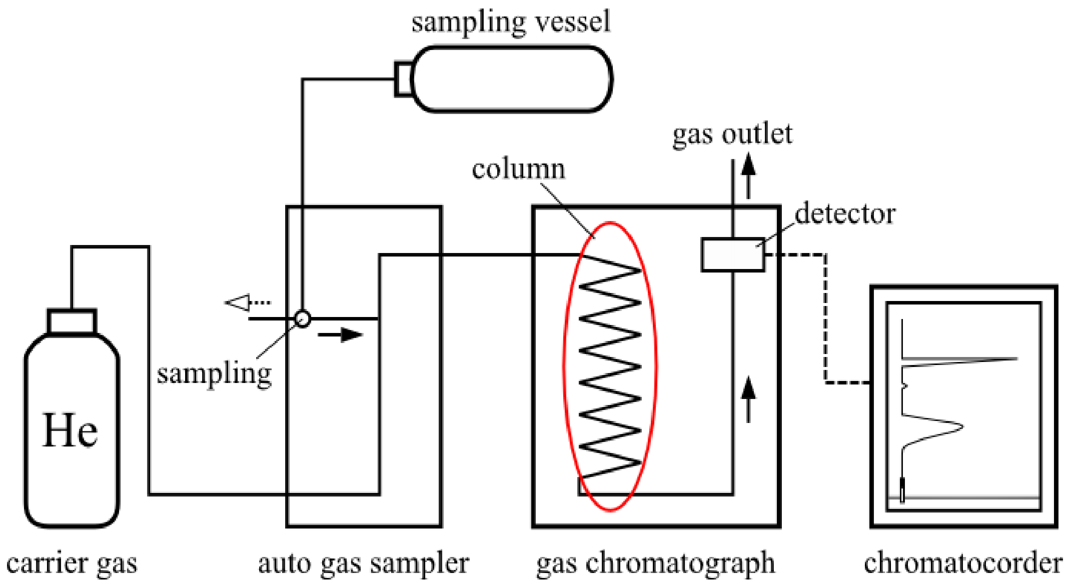

Fig. 2.4 Schematic diagram of gas chromatograph and peripherals

Table 2.8 Setting temperature of each part in gas chromatograph

Refrigerant	Temperature [°C]			Detection time [min]
	Injection	Detector	Column	
R-32/R-1234yf	100	150	120	8
R-32/R-1234yf/CO_2	100	150	75	23
R-125/R-134a/R-143a	100	150	75	23

2.2.4. Measurement of compressor input power and frequency

The power input to the inverter and compressor is measured by a digital power meter (WT1806E, YOKOGAWA). The power measurement accuracy is ±(0.05% of rdg + 0.05% of rng).

2.2.5. Methods of collecting measurement data

The measurement data sent from each sensor is collected by the data acquisition unit (MX100, YOKOGAWA) and imported into the computer via an Ethernet cable. The data is collected and recorded via the system development software LabVIEW (NATIONAL INSTRUMENTS). After the system became stable, all channels were sampled at 1-second intervals for 1 minute, for a total of 60 times. The measured value for each channel was the average of the sampled values.

2.3. Experimental condition and experimental methods

2.3.1. Experimental condition

Table 2.9 shows the experimental condition in used for analysis of heat transfer in the condenser and evaporator in Chapter.3 The experimental analysis is reported by Kawagita.

Table 2.10 shows the conditions in comparison of experimental results and Simuscape simulative results. The experimental analysis using R32 refrigerant is conducted by Takezato.

In refrigerant mixture, the values are calculated using circulation mass fraction measured by gas chromatography. The experiment is conducted charging every 20~40g to find optimum charge amount that COP become highest. In this study, the experimental results are at optimum charge amount.

Table 2.9 Experimental condition measured by Kawagita

	Heat sink/source tempera [ºC]		Heat load [kW]	Superheat [K]
	Condenser	Evaporator		
AHRI	30→35	12 → 7	1.0 to 1.6	4 (±1)
Refrigeration		4 → -6	0.8 to 1.4	

Table 2.10 Experimental condition measured by Takezato

	Heat sink/source tempera [ºC]		Heat load [kW]	Superheat [K]
	Condenser	Evaporator		
Cooling	30 → 45	20 → 10	1.4 to 2.4	4 (±1)
Heating	20 → 45	15 → 9	1.6 to 2.6	
Low-load Heating	20 → 30	15 → 9	1.6 to 2.6	

2.3.2. Experimental methods

The experiment is conducted in following procedure which is same as Kawagita.

① The refrigerant loop is vacuumed. After vacuuming, the refrigerant dissolved in the refrigeration oil in the compressor may evaporate and cause the pressure rise, so the vacuum is repeated several times at intervals.

② The refrigerant charge is conducted from the port on the low pressure side(inlet of the evaporator). The valve of the refrigerant bottle is opened and The hose is filled with refrigerant, and it is confirmed that the pressure inside the refrigerant bottle is higher than the pressure inside the experimental apparatus. If the pressure in the bottle is lower, the refrigerant will not flow into the apparatus or will flow back. If the pressure in the experimental apparatus is sane or higher than the pressure in the refrigerant bottle, the heat source water in the evaporator is controlled to be below the environment temperature and reduce the pressure. If the pressure in the experimental apparatus still does not decrease sufficiently, the pressure at evaporator side is reduced by operating the compressor. After the above preparations are completed, the valve of the refrigerant filling port is opened and refrigerant is charged in a liquid state.

③ In refrigerant charge, weight of refrigerant bottle is measured before and after charging to the experimental apparatus. The charging method is different between the bottle with and without the siphon tubes. When charging from the bottle with the siphon, liquid-phase refrigerant at the bottom of the bottle can be charged. It can be determined whether the charging refrigerant is liquid or gas by seeing the mass change during the charge. If the change of the refrigerant bottle is small, it means the charging refrigerant is gas-phase since the refrigerant amount in the bottle is small. If there is no siphon tube in the refrigerant bottle, the bottle should be reversed when charging to charge the refrigerant as liquid-phase.

④ After charging, the temperature and flow rate of the heat sink/source fluid is set. Specifically, heat source at evaporator side flows 200L/h to prevent freezing. In addition, the electric expansion valve is opened to some extent after fully closing and setting to 0.

⑤ The compressor inverter is turned on and run 3-5 minutes at 1800rpm.

⑥ The compressor frequency, the pulse of the expansion valve, and flow rate of the heat sink/source are adjusted to set the experimental condition. If the refrigerant mass flow rate is not stable, lack of charging amount can be considered. In that case, additional refrigerant is charged.

⑦ After refrigerant flow rate and other measured data become stable under the set experimental results, the temperature, pressure, flow rate, power input to the inverter and the compressor, and the compressor frequency are measured for 3 minutes and recorded.

To find the optimum charge amount that COP becomes highest, every 20~50g refrigerant is charged and set to the condition in process ④-⑦

2.4. Methods of organizing experimental data

The property of the refrigerant and heat sink/source water is estimated using REFPROP Ver. 10.0[10]

2.4.1. Calculation of compressor efficiency

The adiabatic efficiency η_{adi}, mechanical efficiency η_{M}, and volumetric efficiency η_{vol} are calculated as follows.

$$\eta_{\mathrm{adi}} = \frac{h_{\mathrm{d,ideal}} - h_{\mathrm{s}}}{h_{\mathrm{d}} - \mathrm{h_s}} \tag{2.1}$$

$$\eta_{\mathrm{M}} = \frac{m_{\mathrm{R}}(h_{\mathrm{d}} - h_{\mathrm{s}})}{E_{\mathrm{Comp}}} \tag{2.2}$$

$$\eta_{\mathrm{vol}} = \frac{m_{\mathrm{R}}}{\rho_{\mathrm{R,s}} \cdot N \cdot v_{\mathrm{Comp}}} \tag{2.3}$$

where h_{s} and h_{s} are specific enthalpy of compressor inlet and outlet, $h_{\mathrm{d,ideal}}$ is ideal specific enthalpy at compressor discharge, m_{R} is refrigerant mass flow rate, E_{COMP} is power input to the compressor, $\rho_{\mathrm{R,s}}$ is refrigerant density at compressor inlet, N is compressor rotation speed, v_{COMPR} is compressor cylinder volume.

2.4.2. Calculation of heat exchange amount

Heat exchange amount of evaporator and condenser side $Q_{\mathrm{H,Evap}}$ and $Q_{\mathrm{H,Cond}}$ are derived as follows.

$$Q_{\mathrm{H,Evap}} = m_{\mathrm{H,Evap}} \cdot C_{\mathrm{p\ H,Evap}}(T_{\mathrm{H,Evap,in}} - T_{\mathrm{H,Evap,out}}) + Q_{\mathrm{LOSS}} \tag{2.4}$$

$$Q_{\mathrm{H,Cond}} = m_{\mathrm{H,Cond}} \cdot C_{\mathrm{p\ H,Cond}}(T_{\mathrm{H,Cond,in}} - T_{\mathrm{H,Cond,out}}) + Q_{\mathrm{LOSS}} \tag{2.5}$$

where $m_{\mathrm{H,Evap}}$ and $m_{\mathrm{H,Cond}}$ are heat sink/ source mass flow rate which is derived by product of measured volumetric flow rate and density of heat source at heat exchanger inlet. $C_{\mathrm{p\ H,Evap}}$ and $C_{\mathrm{p\ H,Cond}}$ are average constant pressure heat specific heat, and $T_{\mathrm{H,Evap,in}}$, $T_{\mathrm{H,Evap,out}}$, $T_{\mathrm{H,Cond,in}}$, and $T_{\mathrm{H,Cond,out}}$ are heat source temperature at inlet and outlet of evaporator and condenser. Q_{LOSS} is the heat loss caused by the temperature difference between tthe heatsink/source and environment air and corrected before the experiment. The density and constant pressure specific heat of heat sink/source are calculated as follows.

$$\rho_{\mathrm{W}} = a_4 T_{\mathrm{W}}^4 + a_3 T_W^3 + a_2 T_W^2 + a_1 T_{\mathrm{W}} + a_0 \tag{2.6}$$

$$\rho_{\mathrm{B}} = b_4 T_B^4 + b_3 T_B^3 + b_2 T_B^2 + b_1 T_B + b_0 \tag{2.7}$$

$$C_{\mathrm{p\,W}} = c_5 T_W^5 + c_4 T_W^4 + c_3 T_{\mathrm{W}}^3 + c_2 T_W^2 + c_1 T_{\mathrm{W}} + c_0 \tag{2.8}$$

$$C_{\mathrm{p\,B}} = d_5 T_{\mathrm{B}}^5 + d_4 T_{\mathrm{B}}^4 + d_3 T_{\mathrm{B}}^3 + d_2 T_{\mathrm{B}}^2 + d_1 T_{\mathrm{B}} + d_0 \tag{2.9}$$

Equation (2.6) and (2.7) are the approximate equations derived by density and constant pressure specific heat of water at pressure 689.5 kPa in the temperature range 0°C to 100°C, generated from REFPROP Ver. 9.1 [11]. Equation (2.8) and (2.9) are the approximate equations derived by density and constant pressure specific heat in the temperature range -30°C to 160°C, -7.5°C～77.5°C.

Table 2.11 Coefficient of approximate equation in density and constant pressure specific heat of heat sink/source

Approximate equation coefficient of density				Approximate equation coefficient of constant pressure specific heat			
Water		Antifreeze		Water		Antifreeze	
a_4	$-1.2556 \cdot 10^{-7}$	b_4	$2.1064 \cdot 10^{-7}$	c_5	$-3.2220 \cdot 10^{-11}$	d_5	$3.9062 \cdot 10^{-11}$
a_3	$4.0229 \cdot 10^{-5}$	b_3	$-2.6602 \cdot 10^{-5}$	c_4	$1.0770 \cdot 10^{-8}$	d_4	$-5.4451 \cdot 10^{-9}$
a_2	$-7.3948 \cdot 10^{-3}$	b_2	$3.6086 \cdot 10^{-4}$	c_3	$-1.3901 \cdot 10^{-6}$	d_3	$6.3920 \cdot 10^{-8}$
a_1	$4.6734 \cdot 10^{-2}$	b_1	-0.66932	c_2	$9.4433 \cdot 10^{-5}$	d_2	$-4.7348 \cdot 10^{-11}$
a_0	1000.2	b_0	1121.2	c_1	$-3.1103 \cdot 10^{-3}$	d_1	$5.9417 \cdot 10^{-11}$
				c_0	4.2160	d_0	2.6005

Heat exchange amount of evaporator and condenser side $Q_{\mathrm{Ref,Evap}}$ and $Q_{\mathrm{Ref,Cond}}$ are derived as follows.

$$Q_{\mathrm{Ref,Evap}} = m_{\mathrm{Ref}}(h_{\mathrm{Ref,Evap,out}} - h_{\mathrm{Ref,Evap,in}}) \tag{2.10}$$

$$Q_{\mathrm{Ref,Cond}} = m_{\mathrm{Ref}}(h_{\mathrm{Ref,Cond,in}} - h_{\mathrm{Ref,Cond,out}}) \tag{2.11}$$

It is confirmed that the heat balance, the ration of heat exchange amount of refrigerant and heat sink/source side is within 3% in Heating, Low-load Heating, Cooling, and AHRI conditions by Takezato and within 7% in Refrigeration condition by Kawagita.

2.4.3. Calculation of coefficient of performance

The cooling cycle COP $COP_{\mathrm{c,cycle}}$ and the heating cycle COP $COP_{\mathrm{h,cycle}}$ is calculated as follows.

$$COP_{\mathrm{c,cycle}} = \frac{Q_{H,\mathrm{Evap}}}{W_{Comp}} = \frac{Q_{H,\mathrm{Evap}}}{m_{Ref}(h_d - h_s)} \tag{2.12}$$

$$COP_{\mathrm{h,cycle}} = \frac{Q_{H,\mathrm{Cond}}}{W_{Comp}} = \frac{Q_{H,\mathrm{Cond}}}{m_{\mathrm{Ref}}(h_d - h_s)} \tag{2.13}$$

where W_{Comp} is compressor work to the refrigerant. The COP is derived by heat exchange amount of heat sink/source side to refrain from the influence of refrigerant property.

2.4.4. Calculation of overall thermal conductance

The overall thermal conductance *UA* is the product of the overall heat transfer coefficient *U* and heat exchange area *A*. The *UA* is calculated as follows.

$$UA_{Evap} = \sum \frac{Q_{Evap}}{LMTD_{Evap}} \tag{2.14}$$

$$UA_{Cond} = \sum \frac{Q_{Cond}}{LMTD_{Cond}} \tag{2.15}$$

where LMTD is the logarithmic mean temperature difference between refrigerant and heat sink/source.

3. Evaluation of heat transfer coefficient correlation

In this section, the evaporation and condensation heat transfer correlations are compared to consider the influence of the heat transfer model on the simulation results. In the Simscape block, the Gnielinski correlation is used for the single-phase heat transfer coefficient, and the Cavallini and Zecchin correlation is used for the two-phase heat transfer coefficient. It is important to use appropriate correlation according to the refrigerant and heat exchanger. Therefore, the heat exchange in the evaporator and condenser is simulated to evaluate the heat transfer coefficient correlation.

3.1. Heat transfer calculation in double-pipe heat exchanger

Fig. 3.1 shows the schematic diagram of the double-pipe heat exchanger. In the calculation of the heat exchange, the initial input is the property of the refrigerant input and heat sink/source outlet, refrigerant mass flow rate, and heat sink/source volumetric flow rate. It is assumed the heat exchanger is fully insulated. The calculation is conducted by dividing into 1000 segments. The overall thermal conductance UA_{Evap} and UA_{Cond} are calculated in eqation (2.14) and (2.15) respectively.

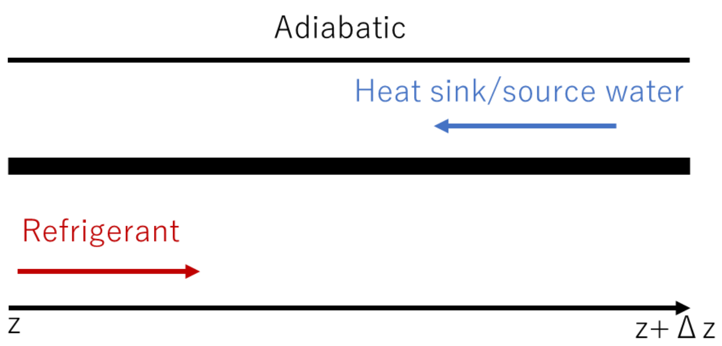

Fig. 3.1 Schematic diagram of heat exchanger

The overall thermal resistance and heat exchange amount is calculated as follows.

$$R = \frac{1}{\Delta UA} = \frac{1}{HTC_{Ref}A_i} + \frac{1}{2\pi k dx} ln\frac{R_0}{R_i} + \frac{1}{HTC_H A_0} \tag{3.1}$$

$$\Delta Q = \frac{|T_H - T_{Ref}|}{R} \tag{3.2}$$

where the HTC is the heat transfer coefficient, and A is the heat exchange area.

The wall temperature is derived as follows.

$$T_{wall} = \frac{HTC_{Ref}R_i T_{Ref} + HTC_H R_H T_H}{HTC_{Ref}R_i + HTC_H R_H} \tag{3.3}$$

The pressure drop of the refrigerant is simplified to be linear to the flow length using the experimental results.

3.2. Heat transfer coefficient correlation

The heat transfer coefficient of the single-phase refrigerant and heat sink/source water is derived from the Gnielinski correlation. This is the same as the correlation used in Simscape block, "Pipe(2P)" and "Pipe(TL)".

$$Nu = \frac{\frac{f}{8}(Re - 1000)Pr}{12.7\sqrt{\frac{f}{8}}(Pr^{2/3} - 1)} \tag{3.4}$$

/

f is the friction factor calculated as follows:

$$f = \{-1.8\log_{10}[\frac{6.9}{Re} + \left(\frac{\varepsilon_r}{3.7}\right)^{1.11}]\}^{-2} \tag{3.5}$$

where ε_r is the roughness of the pipe.

In two-phase refrigerant, the correlations for evaporation and condensation heat transfer coefficient in microfin-tube are suggested by Cavallini(1999)[12] and Cavallini(2009)[13] respectively.

In a zeotropic refrigerant mixture, mass transfer resistance happens during evaporation and condensation due to the difference of the boiling temperature between the components. In R454C and R455A, the heat transfer coefficient correlation with Silver-Bell Ghaly correction for condensation heat transfer and Shah correction for evaporation heat transfer are evaluated by Kim et al[14] [15].

The Silver-Bell Ghaly correction is as follows.

$$HTC_{mixture} = \{\frac{1}{HTC_{pure}} + \frac{Y}{h_v}\}^{-1}$$

$$Y = xc_p\frac{\Delta T_{gl}}{h_{lv}} \tag{3.6}$$

where HTC_{pure} is the heat transfer coefficient derived by the correlation for pure and azeotropic mmixture ΔT_{gl} is the saturation temperature glide, h_{lv} is the latent heat.

The h_v is the heat transfer coefficient correlation derived by following the Dittus-Boelter type correlation.

$$h_v = 0.023{Re_v}^{0.8}{Pr_v}^{0.33}\frac{k_v}{D} = 0.023(\frac{GDx}{D})^{0.8}{Pr_v}^{0.33}\frac{k_v}{D} \tag{3.7}$$

Many evaporation heat transfer correlations consist of the nucleate boiling term and the convective boiling term. In Shah correlation, the nucleate boiling term is corrected with the factor F_c proposed by Thome and Shaki and convective boiling term is corrected by Silver-Bell Ghaly correction.

The Shah correction is as follows.

$$HTC_{mixture} = F_cHTC_{NB} + \{\frac{1}{HTC_{CB}} + \frac{Y}{h_v}\}^{-1} \tag{3.8}$$

where HTC_{NB} is the nucleate boiling term of the existing correlations and HTC_{CB} is the convective boiling term.

In the Simscape model, the Cavallini and Zecchin correlation is used as the default correlation. The correlation is for condensation heat transfer in annular flow based on the Dittus-Boelter correlation.

The Cavallini and Zecchin correlation is as follows[16].

$$HTC = 0.05[\left(\frac{\rho_V}{\rho_L}\right)^{0.5}\left(\frac{\mu_V}{\mu_L}\right)Re_V + Re_L]^{0.8}Pr_L^{0.33}\frac{\lambda_L}{D}$$

$$(= 0.05[(1 - x + x\left(\frac{\rho_L}{\rho_V}\right)^{0.5})Re_{LO}]^{0.8}Pr_L^{0.33}\frac{\lambda_L}{D}) \tag{3.9}$$

$$where\ \ Re_L = \frac{(1-x)GD}{\mu_L}, Re_V = \frac{xGD}{\mu_V}, Re_{LO} = \frac{GD}{\mu_L}$$

In this chapter, the heat transfer characteristics of the refrigerants are analyzed. In addition, the correlations are applied to several refrigerants to evaluate the prediction accuracy of the overall thermal conductance.

Table 3.1 Cavallini(1999) correlation for evaporation heat transfer coefficient

Author	Published	Refrigerant	Suggested correlation
Cavallini, A. [2] Del Col, D. Doretti, L. Longo, G.A. Rossetto, L.	1998	R12 R22 R123 R134a	Evaporation d_t=3.0mm~14.2mm G=90~600kg/(m^{2}s) $\alpha = \alpha_{nb} + \alpha_{cv}$ $\alpha_{nb} = \alpha_{Cooper} S F_1(d_i)$ $= [55{P_R}^{0.12}(-log_{10}(P_r))^{-0.55} M^{-0.5} q_{en}^{0.67}] S F_1(d_i)$ $q_{en} = \alpha_{nb}(T_w - T_s)$ $S = A{X_{tt}}^B = A[(\frac{1-x}{x})^{0.9}\left(\frac{\rho_V}{\rho_L}\right)^{0.5}\left(\frac{\mu_V}{\mu_L}\right)^{0.1}]^B$ *if X_{tt}>1 then X_{tt}=1* $F_1(d_i) = (\frac{d_0}{d_t})^c$ $\alpha_{cv} = \frac{\lambda_L}{d_t} Nu_{cv,smooth\ tube} Rx^S (BoFr)^T F_2(d_i) F_3(S)$ $Nu_{cv,smooth\ tube} = Nu_{LO} F$ $= [0.023\left(\frac{Gd_t}{\mu_L}\right)^{0.8} Pr^{\frac{1}{3}} \times \{\left[(1-x) + 2.63x\left(\frac{\rho_L}{\rho_V}\right)^{\frac{1}{2}}\right]^{0.8}$ $Pr_L = \frac{\mu_L c_{pL}}{\lambda_L}$ $Rx = \{[2h_{fin} n_g\left(1 - \sin\left(\frac{\gamma}{2}\right)\right)]/[\pi d_t \cos\left(\frac{\gamma}{2}\right)] + 1\}/\cos(\beta)$ $Bo = g\rho_L h_{fin} d_t/(8\sigma n_g)$ $Fr = {u_{VO}}^2/(gd_t)$ $F_2(d_i) = (\frac{d_0}{d_t})^V, d_0 = 0.01m$

			$F_3(G) = \left(\frac{G_0}{G}\right)^Z, G_0 = 100kg/(m^2s)$

	A	B	C	S	T	V	Z	d_0 (m)	G_0 kg/(m^{2}s)
G<500 kg/(m^2· s)	1.36	0.36	0.38	2.14	-0.15	0.59	0.36	0.01	100
G≥500 kg/(m2· s)	1.36	0.36	0.38	2.14	-0.21	0.59	0.36	0.01	100

Table 3.2 Cavallini(2009) for condensation heat transfer coefficient

Author	Published	Refrigerant	Suggested correlation
A.Cavallini[28]	2009	R22	Condensation
		R134a	d_t=5.95mm~14.18mm
D.Del.Col		R123	G=80~910kg/(m^{2}s)
S.Mancin		R410A	
L.Rossetto		CO2	$\alpha = ({\alpha_A}^3 + {\alpha_D}^3)^{0.333}$
			$\alpha_A = \alpha_{AS} A * C$
			$\alpha_{AS} = \alpha_{LO}[1 + 1.128x^{0.817}\left(\frac{\rho_L}{\rho_V}\right)^{0.3685}\left(\frac{\mu_L}{\mu_G}\right)^{0.2363}$
			$-\frac{\mu_G}{\mu_L}\Big)^{2.144} Pr_L^{-0.1}]$
			$\alpha_{LO} = 0.023\frac{\lambda_L}{d_t}\left(\frac{Gd_t}{\mu_L}\right)^{0.8} Pr_L^{-0.4}$
			$Fr = \frac{G^2}{gd_t(\rho_L - \rho_V)^2}$
			$A = 1 + 1.119Fr^{-0.3821}(Rx - 1)^{0.3586}$
			$Rx = \left\{\frac{2h_{fin}n_g\left(1 - \sin\left(\frac{\gamma}{2}\right)\right)]}{\pi d_t \cos\left(\frac{\gamma}{2}\right)} + 1\right\}\frac{1}{\cos(\beta)}$
			$C = 1, if \ \ (N_{opt}/N) \geq 0.8$
			$C = \ \ (N_{opt}/N)^{1.904}, if \ \ (N_{opt}/N) < 0.8$
			$N_{opt} = 4064.4d_t + 23.257$
			$\alpha_D = C\{2.4x^{0.1206}(Rx - 1)^{1.466}C_1^{0.6875} + 1\}\alpha_{D,S}$
			$\alpha_{D,S} = \frac{0.725}{1 + 0.741\left(\frac{1-x}{x}\right)^{0.3321}}\left[\frac{\lambda^3\rho_L(\rho_L - \rho_V)g * h_{LG}}{\mu_L D * \Delta T}\right]^{0.25}$
			$C_1 = 1, if \ \ J_G \geq {J_G}^*$
			$C_1 = (J_G/{J_G}^*), if \ \ J_G < {J_G}^*$

			$J_G{}^* = 0.6\left[\left\{\frac{7.5}{4.3X_{tt}{}^{1.111}+1}\right\}^{-3} + 2.5^{-3}\right]^{-0.3333}$

3.1. Condition and refrigerants

Table 3.3 shows the experimental condition and refrigerants that heat transfer in the evaporator and condenser is analyzed. In AHRI condition, R32/R1234yf (22/78 mass%) and R32/R1234yf/CO_2(22/72/6 mass%) are measured by Takezato and R404A and R32/R1234yf/CO_2 (22/74/4 mass%) are measured by Kawagita. The Refrigeration condition is measured by Kawagita and Cooling condition is measured by Takezato. In Refrigeration condition, only condenser side is analyzed because the property of the heat source antifreeze is not known except for density and specific heat.

In evaporation heat transfer, Cavallini(1999) correlation with and without the Shah correction are applied and Cavallini(2009) correlation with and without the Silver-Bell Ghaly correction is applied to refrigerant mixtures. In Cooling condition, the Cavallini and Zecchin correlation is applied to both of the evaporation and condensation heat transfer to evaluate prediction accuracy and influence to Simscape simulation.

Table 3.3 Simulative conditin and refrigerants

<table>
<tr><th></th><th>Refrigerant</th></tr>
<tr><td>AHRI</td><td rowspan="2">・R404A
・R32/R1234yf (22/78 mass%)　(≒R454C)
・R32/R1234yf/CO2(22/74/4 mass%)　(≒R455A)
・R32/R1234yf/CO2(22/72/6 mass%)</td></tr>
<tr><td>Refrigeration
(Only condenser side)</td></tr>
<tr><td>Cooling</td><td>・R32
・R32/R1234yf (22/78 mass%)</td></tr>
</table>

3.3. Results in AHRI and Refrigeration condition

3.3.1. Condensation heat transfer

Fig.3.2 shows the heat transfer coefficient of the refrigerant in the condenser. The heat transfer coefficient decreases as the CO_2 mass fraction increases since the mass transfer resistance due to the temperature glide increases.

Fig.3.4 shows the prediction accuracy of the overall thermal conductance UA in the condenser side. If the prediction error is big, the refrigerant temperature cannot be simulated accurately in the simulation because the logarithmic mean temperature difference changes for the same heat exchange amounts. The prediction error is within 15% in AHRI condition and within 30% in the Refrigeration condition. The error is bigger as the CO_2 mass fraction increases. And the error is bigger if the correction for the heat transfer coefficient correlation is not applied. The prediction improved 6.1 % in AHRI condition and 6.4% in refrigeration condition at max.

In both the evaporator and condenser side, the prediction error increases as the CO_2 mass fraction increases and the prediction accuracy improve about 5~6% by applying the Shah correction and the Silver-Bell Ghaly correction to the existing heat transfer coefficient correlation.

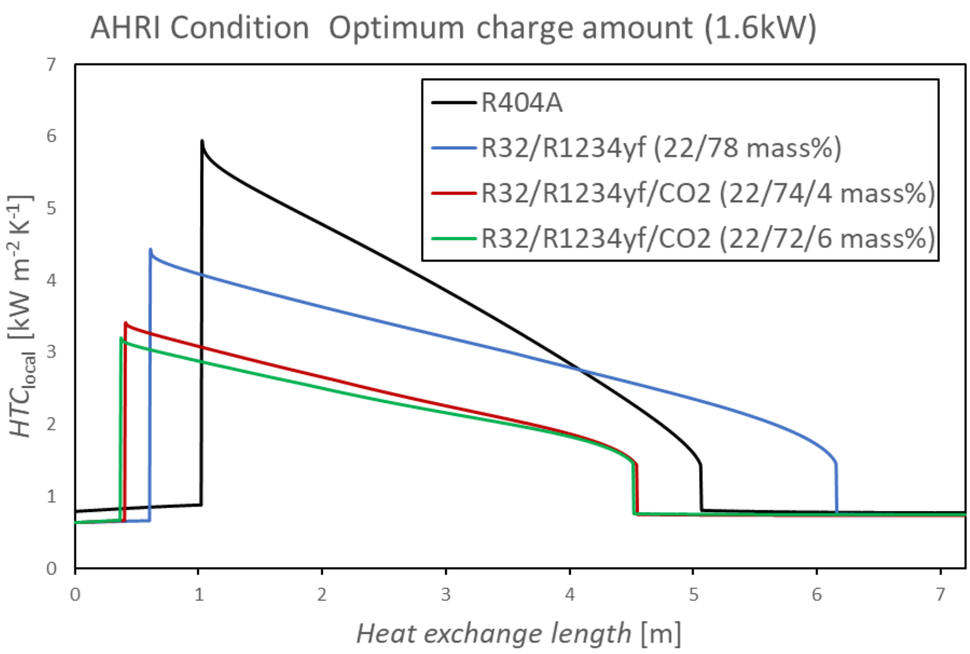

Fig. 3.2 Distribution of heat transfer coefficient in condenser (AHRI 1.6kW)

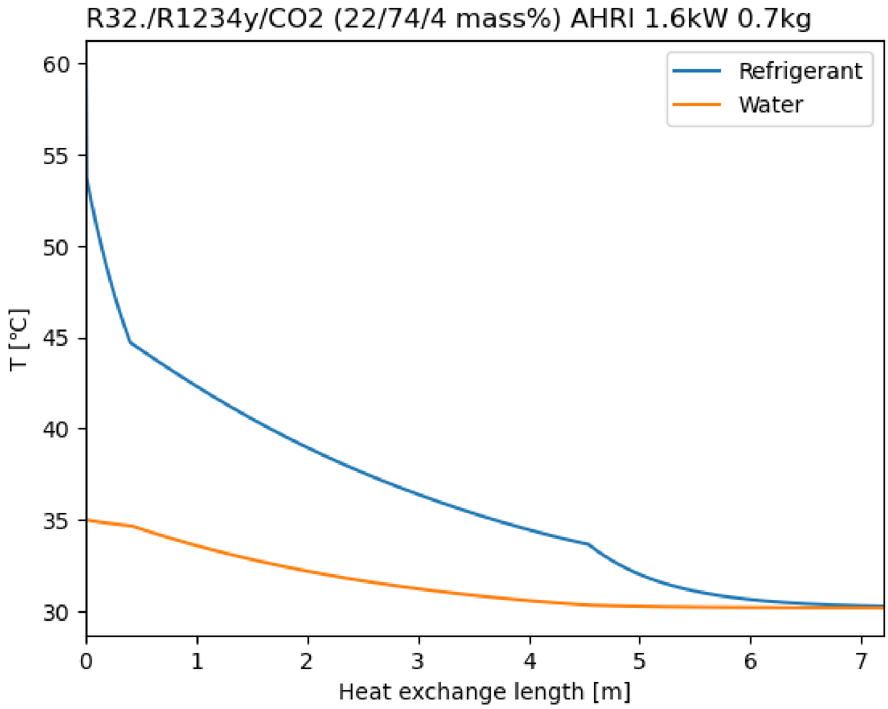

Fig. 3.3 Temperature distribution of refrigerant and heat sink water (AHRI 1.6kW)

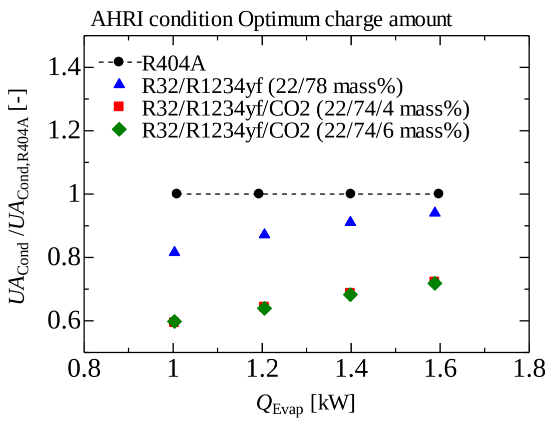

(a)AHRI condition

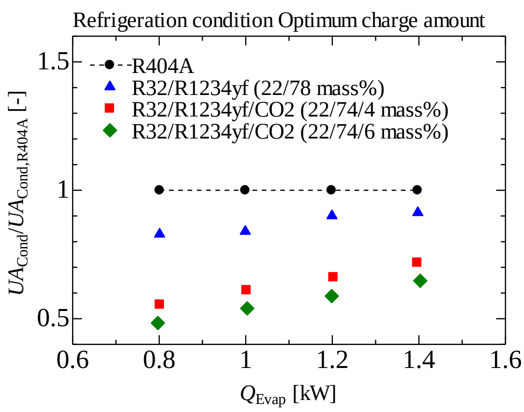

(b) Refrigeration condition

Fig. 3.4 Experimental relative UA to R404A in condenser

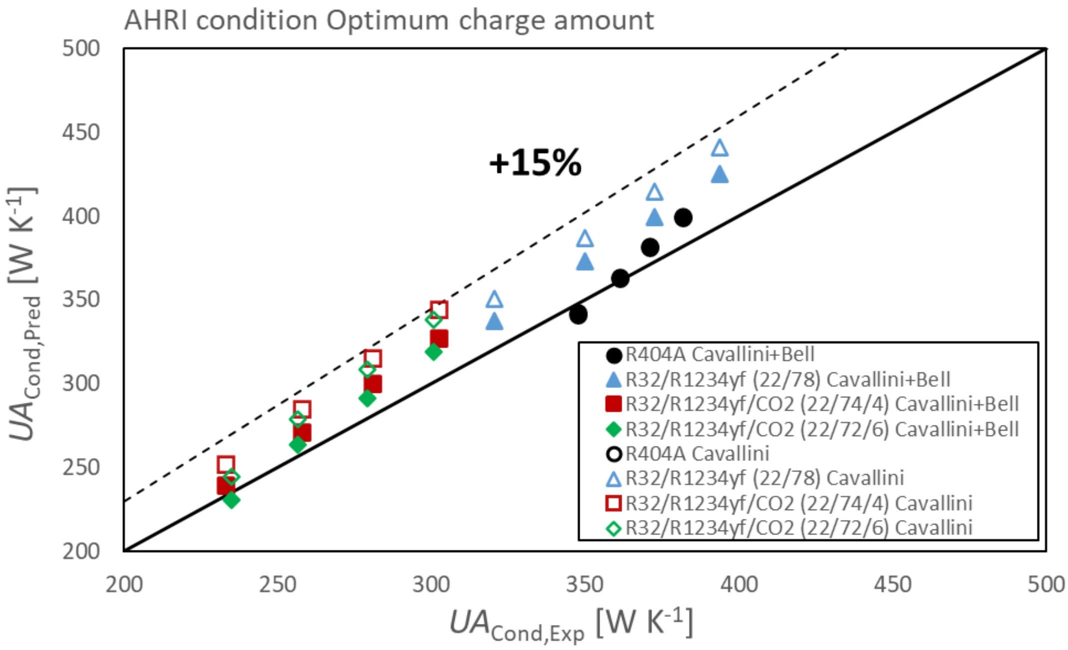

(a) AHRI condition

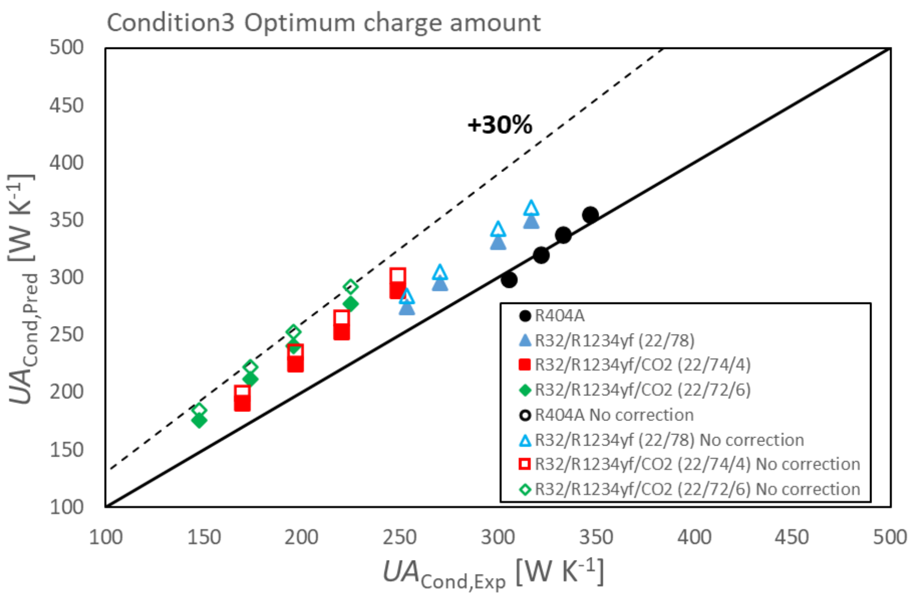

(b) Refrigeration condition

Fig. 3.5 Comparison of condensation UA between experiment and simulation

3.3.2. Evaporation heat transfer

Fig. 3.6 shows the predicted heat transfer coefficient distribution in AHRI condition 1.0kW. In the prediction with the correction, heat transfer coefficient is lower as the CO_2 mass fraction increases as well as the evaporation heat transfer coefficient In addition, the heat transfer coefficient of R32/R1234yf/CO_2(22/74/4 mass%) and R32/R1234yf/CO_2(22/72/6 mass%) decreases. In general, the evaporation heat transfer coefficient increases as vapor quality increases. However, if the temperature glide is higher than the heat source temperature difference, the temperature difference between the refrigerant and heat source water decreases as heat exchange proceeds as shown in Fig. 3.7. That suppresses heat transfer and the heat transfer coefficient decreases. Fig. 3.8 (a), (b) shows experimental relative UA to R4040A in AHRI condition and Refrigeration condition. In Refrigeration condition, the heat source temperature difference is 10K, higher than that in AHRI condition 5K and the overall thermal conductance UA of refrigerant mixtures in refrigeration condition are closer to that of R404A in AHRI condition since heat transfer is not suppressed and the temperature glide works effectively. In addition, the UA of the zeotropic mixtures is close to that of R404A as heat load increases in both of the condenser and evaporator side. This is because as heat load increases, the refrigerant mass flow rate increases. In zeotropic mixture, the fraction of the component is different between liquid and vapor phase during the phase change because the boiling temperature is different. That causes the temperature gradation in the radial direction and contributes to decreasing effective temperature difference for heat transfer(Mass transfer resistance). But as refrigerant mass flow rate increases, the refrigerant is mixed more and the resistance decreases. Therefore, the UA is close to that of R404A.

Fig. 3.9 shows the prediction accuracy of the overall thermal conductance UA in evaporator side. R404A 1.0-1.4kW are removed since the refrigerant is still two-phase in the simulation. In the zeotropic mixture, the UA is predicted within 30%, but the prediction error is bigger as UA increases, meaning the heat load increases. And the error is bigger as the CO_2 mass fraction increases as well as the condenser side. The UA is also predicted without the Shah correction. The error of the UA prediction without the Shah correction is bigger than that with the Shah correction. As shown in Fig. 3.10 the heat transfer coefficient is predicted higher if the correction is not applied and cause the prediction error to increase. In AHRI condition, the prediction accuracy improves 5.3% at max with the Shah correction.

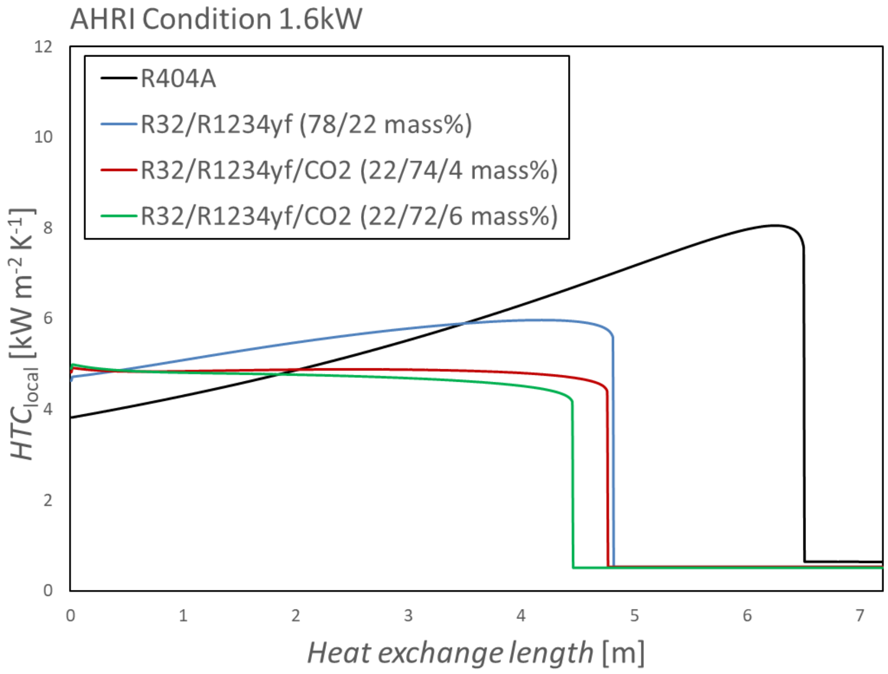

Fig. 3.6 Distribution of predicted heat transfer coefficient (AHRI, 1.6kW)

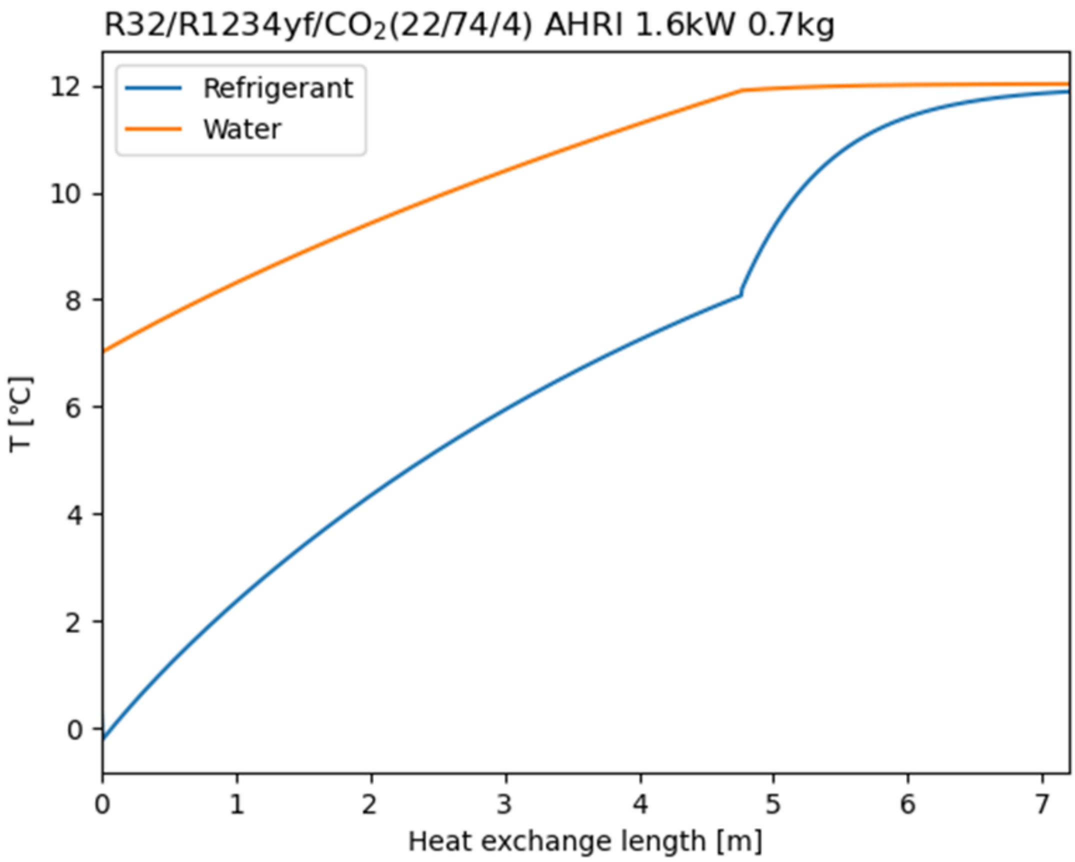

Fig. 3.7 Temperature distribution of the refrigerant and heat source water in evaporator

($R32/R1234yf/CO_2$(22/74/4 mass%) AHRI condition 1.6kW)

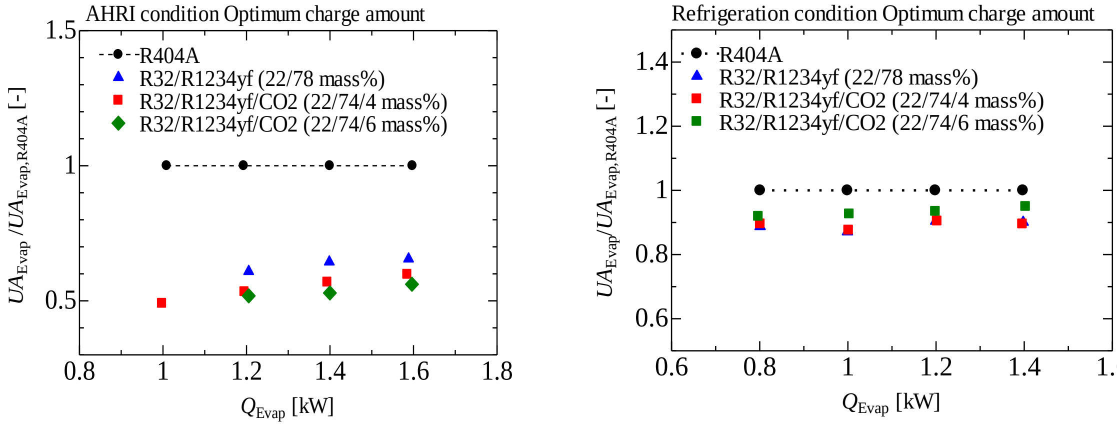

(a)AHRI condition (b) Refrigeration condition

Fig. 3.8 Experimental relative UA to R404A in evaporator

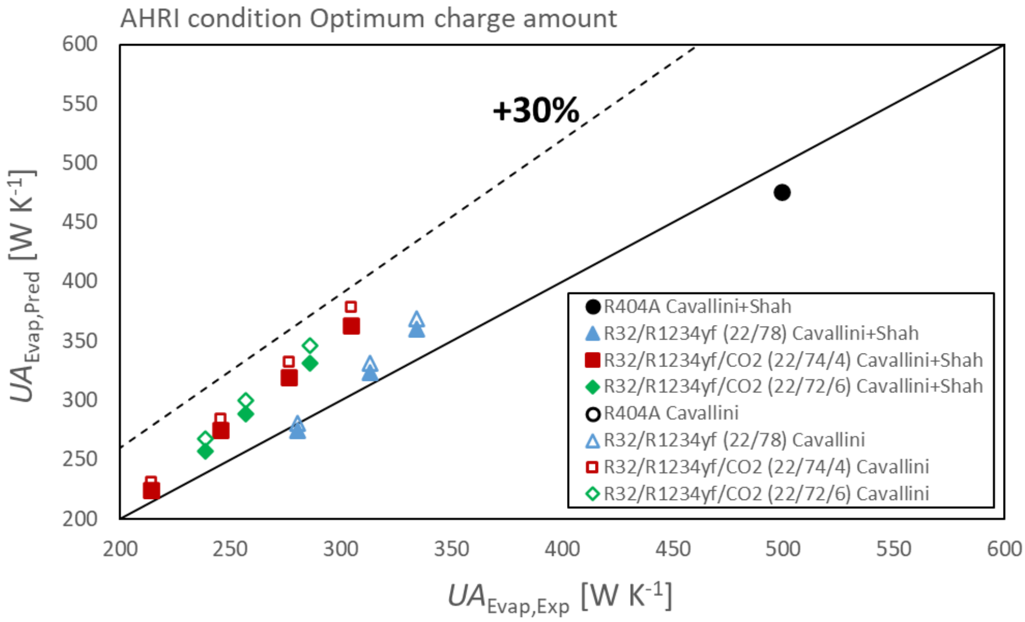

Fig. 3.9 Comparison of evaporation UA between experiment and simulation

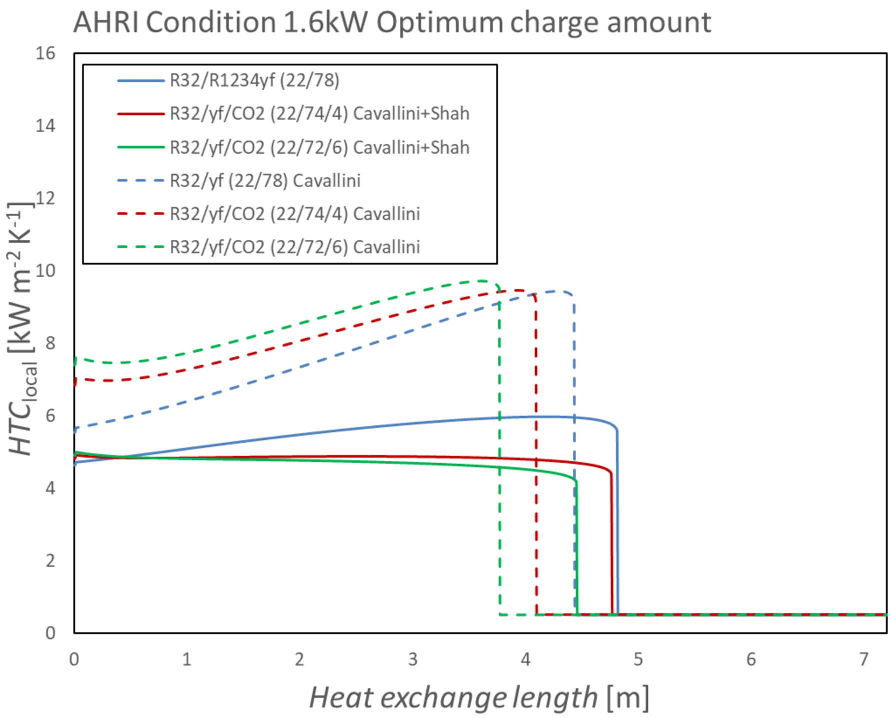

Fig. 3.10 Comparison of heat transfer coefficient with and without the correction

3.5. Condensation heat transfer in Cooling condition

In chapter.4, the heat pump cycle simulation is compared with the experiment in the Cooling condition. In this section, the heat exchange simulation of R32 and R32/R1234yf(22/78 mass%) is conducted using Cavallini(2009) correlation and Cavallini and Zecchin correlation, which is used in Simscape. In this simplified simulation, the heat exchange of R32 in evaporator side is not simulated well since the pinch point is almost zero, so the results of the condenser side is shown. Fig. 3.11 Shows the the heat transfer coefficient distribution of the R32 and R32/R1234yf(22/78 mass%) in the condenser. In R32, the refrigerant is still two-phase in the simulation using the Cavallini and Cavallini and Zecchin correlation. In 2.4kW, the subcooled liquid happens at the condenser outlet. This means that the single-phase and two-phase heat transfer correlation predict lower than actual case. Especially, the Cavallini and Zecchin correlation predict lower since the correlation does not consider the wall subcool. In R32, it is necessary to use a more accurate correlation that does not include the problems described in chapter.4, or to correct the heat exchanger length.

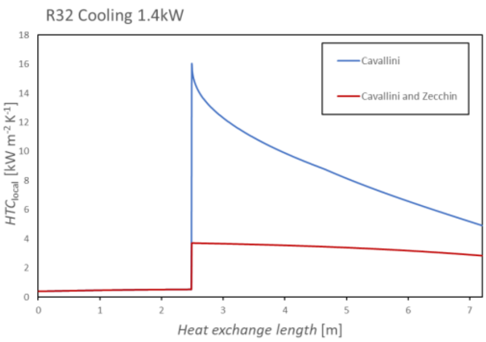

(a) R32 Cooling 1.4kW

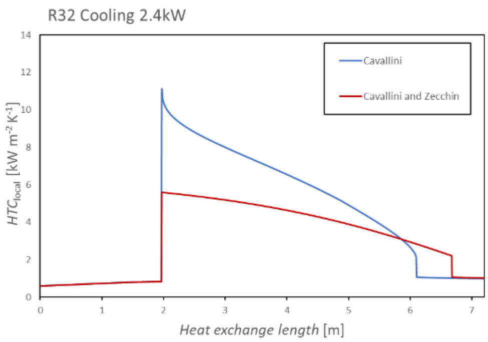

(b) R32 Cooling 24kW

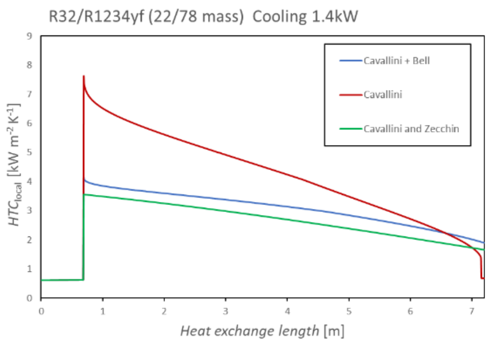

(c) R32/R1234yf(22/78 mass%)

Cooling 1.4kW

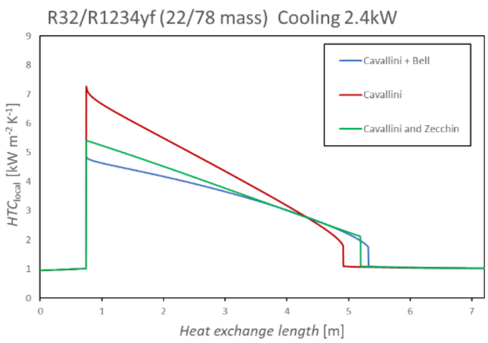

(d) R32/R1234yf(22/78 mass%)

Cooling 1.4kW

Fig. 3.11 Comparison of condensation heat transfer coefficient between the correlations

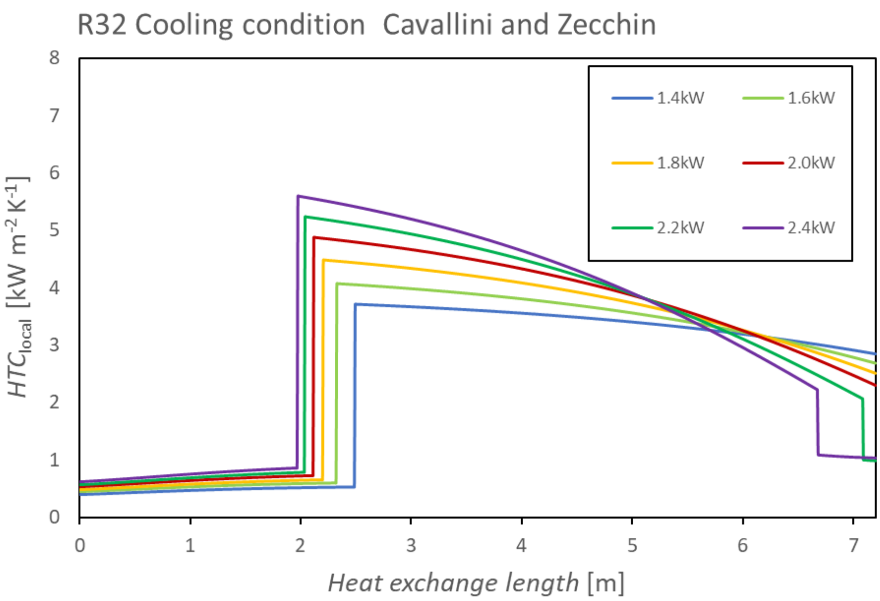

Fig. 3.12 Distribution of heat transfer coefficient

(R32 Cooling Cavallini and Zecchin correlation)

4. Simulative analysis of the heat pump

4.1. Heat pump cycle model in Simscape

Fig. 4.1 shows the block diagram of the heat pump simulation model. The Simscape model uses physical connections and enable to flow bidirectionally between components. The simulation is conducted in MATLAB R2023b environment.

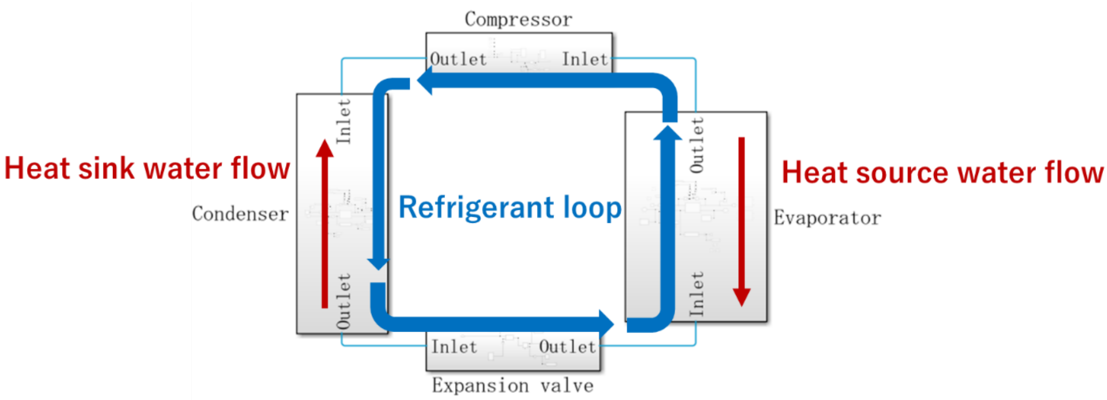

Fig. 4.1 Simulation model in Simscape

4.1.1. Compressor model

Fig. 4.2 shows the compressor model. The scroll compressor is modeled by "Positive-Displacement Compressor(2P)". The angular velocity is calculated in "Ideal Angular Velocity Source" block.

The mass flow rate is calculated as follows.

$$m = \eta_v \omega \frac{V_{disp}}{v_s} \tag{4.1}$$

where m is the mass flow rate, ω is the angular velocity, v_s is the specific volume at the inlet.

The energy balance equation is as follows.

$$\Phi_{\mathrm{in}} + \Phi_{\mathrm{out}} + m_A \Delta h_t = 0 \tag{4.2}$$

where Φ_{in} is energy flow at the inlet, Φ_{out} is energy flow at the outlet, $m_A \Delta h_t$ is the power input to the fluid.

The volumetric efficiency is calculated as follows.

$$\eta_v = 1 + C - C\left(\frac{P_{out}}{P_{in}}\right)^{\frac{1}{n}} \tag{4.3}$$

$$C = \frac{1 - \eta_{v_{norminal}}}{p_{ratio}{}^{\frac{1}{n}} - 1} \tag{4.4}$$

where n is the polytropic exponent and p_{ratio} is nominal pressure ratio.

The power to the fluid is calculated as follows.

$$W_c = \omega \frac{n}{n-1} \eta_{v_{norminal}} V_{disp} [\left(\frac{P_{out}}{P_{in}}\right)^{\frac{n-1}{n}} - 1] \tag{4.5}$$

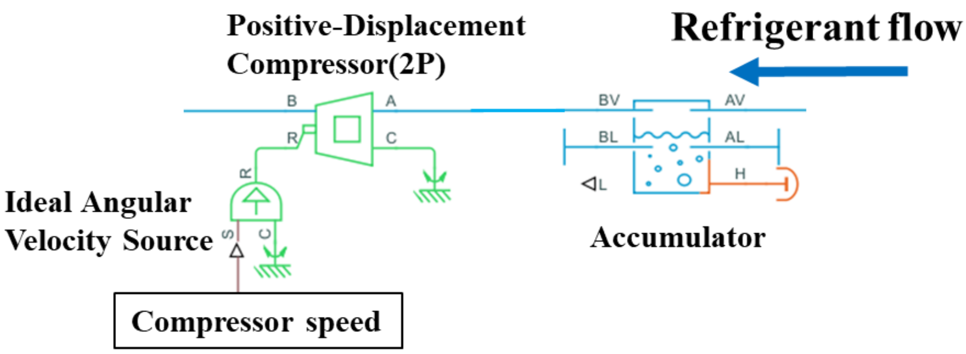

Fig. 4.2 Compressor model

4.1.2. Expansion valve model

Fig. 4.3 shows the expansion valve model. The expansion valve is modeled by "Local Restriction(2P)" block that model pressure drop due to a localized reduction in flow area. The valve opening is controlled by PI control according to the difference from target superheat. The parameter is set as follows.

Table 4.1 Parameters of heat exchanger

A_{*} : $\pi/4D_h^2$ m^2	D_h : 1.65 mm
$A_{R,min}$: $\frac{\pi}{4}(D_h \times 0.9)^2$ m^2	B_L : 0.999
$A_{R,max}$: $\frac{\pi}{4}\left(D_h \times 10^{-4}\right)^2$ m^2	C_D : 0.64

Energy Balance

The energy balance equation is as follows.

$$\Phi_{in} + \Phi_{out} = 0 \tag{4.6}$$

Assuming the expansion is adiabatic process, the enthalpy change is 0. The inlet and outlet can be expressed as follows.

$$u_{*} + P_{*}v_{*} + \frac{w_{*}^2}{2} = u_R + P_R v_R + \frac{w_R^2}{2} \tag{4.7}$$

The subscript ($*$) means the inlet or outlet and (R) means restriction aperture.

The ideal flow velocity is as follows.

$$w_{*} = \frac{\dot{m}_{ideal} v_{*}}{A_{*}} \tag{4.8}$$

$$\dot{m}_{ideal} = \frac{\dot{m}_{in}}{C_D} \tag{4.9}$$

where C_D is the flow discharge coefficient for the local restriction.

Momentum balance

The mass flow rate is derived as follows.

$$\dot{m} = A_{\mathrm{R}}(P_{\mathrm{in}} - P_{\mathrm{out}})\sqrt{\frac{2}{|P_{\mathrm{in}} - P_{\mathrm{out}}|v_{\mathrm{R}}K_{\mathrm{T}}}} \quad (Turbulent\ \ flow)$$

$$\dot{m} = A_{\mathrm{R}}(P_{\mathrm{in}} - P_{\mathrm{out}})\sqrt{\frac{2}{\Delta P_{\mathrm{Th}}v_{\mathrm{R}}\left(1 - \frac{A_{\mathrm{R}}}{A_{*}}\right)^{2}}} \quad (Laminar\ \ flow) \tag{4.10}$$

where K_{T} and ΔP_{Th} are defined as follows.

$$K_{\mathrm{T}} = \left(1+\frac{A_{\mathrm{R}}}{A_{*}}\right)\left(1 - \frac{v_{\mathrm{in}}}{v_{\mathrm{out}}}\frac{A_{\mathrm{R}}}{A_{*}}\right) - 2\frac{A_{\mathrm{R}}}{A_{*}}\left(1 - \frac{v_{\mathrm{out}}}{v_{\mathrm{in}}}\frac{A_{\mathrm{R}}}{A_{*}}\right) \tag{4.11}$$

$$\Delta P_{\mathrm{Th}} = \left(\frac{P_{\mathrm{in}}+P_{\mathrm{out}}}{2}\right)(1 - B_{\mathrm{L}}) \tag{4.12}$$

The pressure at the restriction area is derived as follows.

$$P_{\mathrm{R}} = P_{\mathrm{in}} - \frac{v_{\mathrm{R}}}{2}\left(\frac{\dot{m}}{A_{\mathrm{R}}}\right)^{2}\left(1+\frac{A_{\mathrm{R}}}{A_{*}}\right)\left(1 - \frac{v_{\mathrm{in}}}{v_{\mathrm{out}}}\frac{A_{\mathrm{R}}}{A_{*}}\right) \quad (Turbulent\ \ flow)$$

$$P_{\mathrm{R}} = \frac{P_{\mathrm{in}}+P_{\mathrm{out}}}{2} \quad (Laminar\ \ flow) \tag{4.13}$$

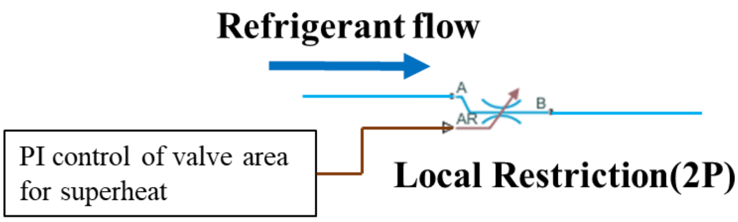

Fig. 4.3 Expansion valve model

4.1.3. Heat exchanger model

Fig. 4.4 shows the evaporator and condenser model. The double-pipe heat exchanger is modeled by connecting "Pipe(2P)" block that refrigerant flows and "Pipe(TL)" blocks that heat sink/source water flows. The heat exchanger is modeled by dividing into 10 segments to improve the calculation accuracy. In addition, there is receiver block at condenser outlet point. The heat sink/source water is supplied from "Reservoir(TL)" tank and volumetric flow rate is controlled by "Flow rate source(TL)" block.

Pipe(2P) and Pipe(TL) bock parameters are set as follows.

.

Table 4.2 Pipe(2P) and Pipe(TL) bock parameters

Pipe(2P) parameter	
L : 1.08 m (divided into 10 segments)	Laminar flow upper Reynolds number limit: 2000
D_h : 7.52 mm	Turbulent flow lower Reynolds number limit: 4000
A : $\frac{\pi}{4}{D_h}^2$ m^2	Nusselt number for laminar flow heat transfer: 3.66
ε_r: 1.5×10^{-6} m	Initial pressure: Follows experimental data
τ: 0.1	Initial vapor quality: Follows divided segments
η_{shape}: 64	
Pipe(TL) parameter (Only the parameters different from Pipe(2P))	
L : 1.08 m (divided into 10 segments)	Initial pressure: Heat sink/source inlet temperature
D_h : (13.88-9.52) mm	A : $\frac{\pi}{4}(13.88^2 - 9.52^2)$ m^2

In both of condenser and evaporator, the Cavallini and Zecchin correlation for condensation heat transfer coefficient is used. The correlation also does not consider enhancement of heat transfer by micro-fin tube. Therefore, the heat exchanger length is 1.5 times longer than actual case because the enhancement of the surface area with the microfin is 1.5 times. In addition, the Cavallini and Zecchin correlation for condensation heat transfer coefficient is also applied to the evaporation heat transfer coefficient. The correlation only consider the convective heat transfer, does not consider the nucleate heat transfer, and will predict the evaporation heat transfer lower.

The detailed explanation about Pipe(2P) is as follows.

Energy balance

The energy balance equation is as follows.

$$Mu_{\mathrm{I}}+(m_{\mathrm{in}}+m_{\mathrm{out}})u=\phi_{\mathrm{in}}+\phi_{\mathrm{out}}+Q \tag{4.14}$$

where M is mass of the fluid, u is specific internal energy.

The heat heat flow rate Q is calculated as follows:

$$Q=HTC\times A(T_H-T_{\mathrm{I}}) \tag{4.15}$$

where HTC is heat transfer coefficient, T_H is pipe wall temperature and T_{I} is fluid temperature.

The heat transfer coefficient is calculated as follows.

$$\begin{aligned} HTC &= \frac{k_I Nu}{D_{\mathrm{h}}} \quad (Single\ \ phase) \\ &= \frac{k_{sat,liq} Nu}{D_{\mathrm{h}}} \quad (Two\ \ phase) \end{aligned} \tag{4.16}$$

In single phase refrigerant and heat sink/source water, the Nusselt number is calculated by Gnielinski correlation. In two phase, the Nusselt number is calculated by Cavallini and Zecchin correlation.

Mass balance

The mass balance equation is as follows.

$$\left[\left(\frac{\partial\rho}{\partial p}\right)_{\mathrm{u}}\dot{P}_{\mathrm{I}}+\left(\frac{\partial\rho}{\partial u}\right)_{\mathrm{p}}\dot{u}_{\mathrm{I}}\right]V=\dot{m}_{\mathrm{in}}+\dot{m}_{\mathrm{out}}+\epsilon_{\mathrm{M}} \tag{4.17}$$

where V is fluid volume, ϵ_{M} is the correction for the smoothing of the density partial derivatives across phase transition boundaries.

The density partial derivatives of the various domains is calculated using a cubic polynomial function. When vapor quality is between 0 and 0.1, the subcooled liquid and two-phase domains are blended. In vapor quality 0.9 – 1.0, the superheated vapor and two-phase domains are blended. ϵ_{M} is derives as follows.

$$\epsilon_{\mathrm{M}} = \frac{M - \frac{V}{v_{\mathrm{I}}}}{\tau} \tag{4.18}$$

The fluid mass in the pipe block is as follows.

$$M = m_{\mathrm{A}} + m_{\mathrm{B}} \tag{4.19}$$

Momentum balance

The momentum balance is calculated for the half piee if the inlet side and the outlet side separately.

$$P_{\star} - P_{\mathrm{I}} = \frac{m_{\star}}{A_{\mathrm{I}}}\left|\frac{m_{\star}}{A_{\mathrm{I}}}(v_{\mathrm{I}} - v_{\star})\right| + F_{\mathrm{vis},\star} + I_{*} \tag{4.20}$$

where I_{*} is the fluid interia calculated as follows.

$$I_{*} = m\frac{L}{2\mathrm{S}} \tag{4.21}$$

In laminar flow, the viscous friction force $F_{\mathrm{visc},\star}$ is calculated as follows:

$$F_{\mathrm{visc},\star} = \frac{f_{\mathrm{shape}} L v_{I} m_{\star}}{4 D_{\mathrm{h}}^{2} A_{\mathrm{I}}} \tag{4.22}$$

f_{shape} is the pipe shape factor.

In turbulent flow, the viscous friction force is calculated as follows.

$$F_{\text{visc},\star} = \frac{\dot{m}_\star |\dot{m}_\star| f_\star L \nu_I}{4D_{\text{h}}^2 A_{\text{I}}} \tag{4.23}$$

$f_\star$ is the Darcy friction factor for turbulent flow.

$$f_\star = \frac{1}{\left\{-1.8\,log_{10}\left[\frac{6.9}{Re_\star} + \left(\frac{\varepsilon_{\text{r}}}{3.7}\right)^{1.11}\right]\right\}^2} \tag{4.24}$$

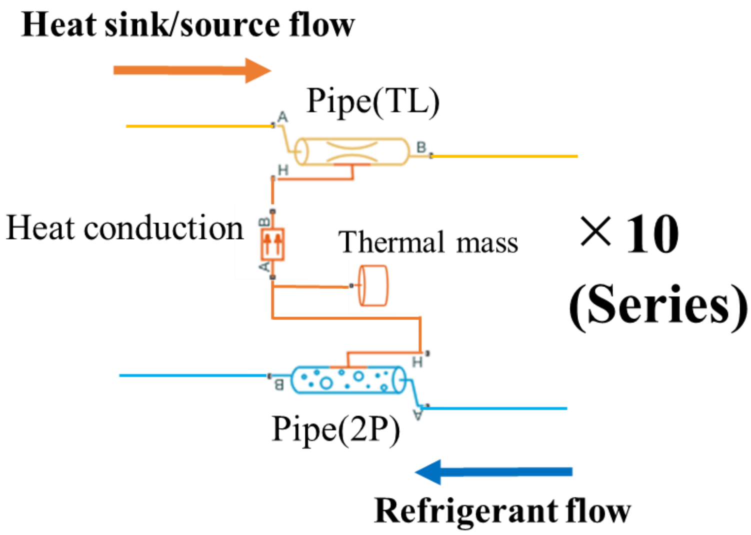

Fig. 4.4 Model of Double-pipe heat exchanger

4.1.4. Accumulator and receiver

There is accumulator block at compressor inlet and receiver block at condenser outlet. The blocks are fully insulated and increase the stability in the cycle. The accumulator is the support block that reproduce the compressor volume and it helps controlling compressor pressure ratio by changing accumulator volume. The receiver block is connected to 1m Pipe(TL) to support reproducing the subcool.

Table 4.3 Parameters of accumulator and receiver

Accumulator parameter	
Accumulator volume: Follows condition	Initial pressure: Follows experimental data

A: $\frac{\pi}{4}(7.52\times10^{-3})^2$ m^2	Initial liquid mass fraction: 0
Receiver parameter	
Receiver volume: 0.001 m^3	Initial pressure: Follows experimental data
A: $\frac{\pi}{4}(7.52\times10^{-3})^2$ m^2	Initial liquid mass fraction: 1
Vapor heat transfer coefficient: 20 W/(K*m^2)	
Liquid heat transfer coefficient: 500 W/(K*m^2)	
Parameter of Pipe(TL) connected to Receiver block	
L : 1 m	Initial pressure: Heat sink/source inlet temperature
D_h : (13.88-9.52) mm	

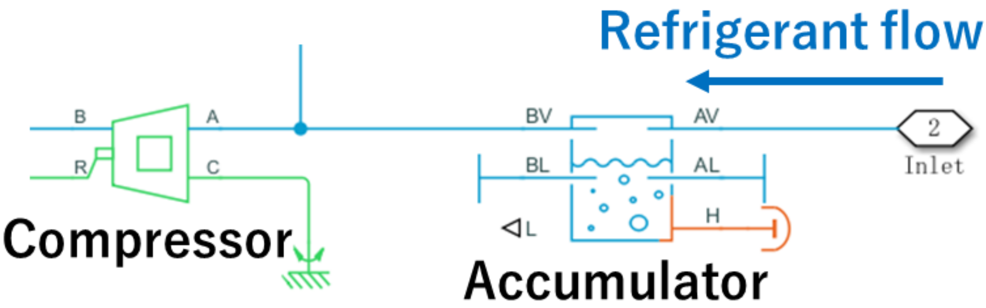

Fig. 4.5 Accumulator model

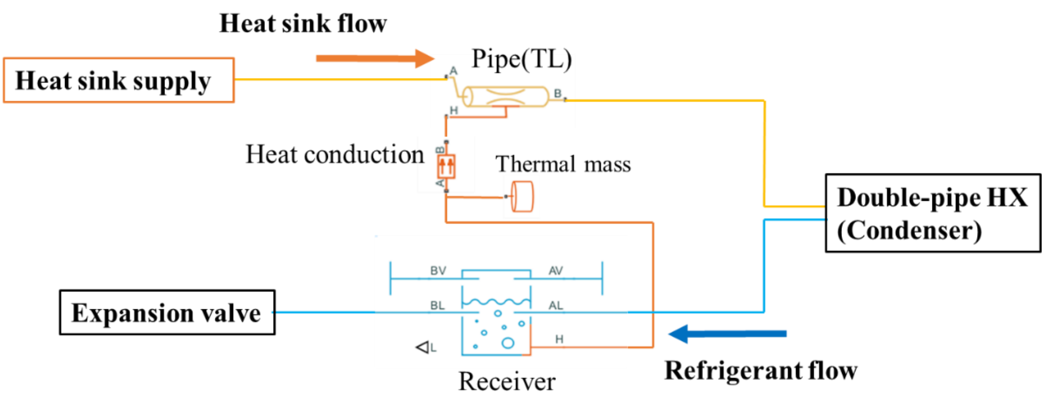

Fig. 4.6 Receiver model

4.1.5. Fluid property, Superheat, and Subcool

The refrigerant property is set using “Two-Phase Fluid Properties (2P)”. The refrigerant property table is made in MATLAB via REFPROP. There are property data of pressure, specific internal energy, temperature, specific entropy, specific volume, kinematic viscosity, Prandtl number of liquid phase and vapor phase. The fluid properties are parameterized in terms of pressure and normalized internal energy as shown in Fig. 4.7.

In subcooled liquid phase, the normalized internal energy is defined as follows.

$$\bar{u} = \frac{u - u_{min}}{u_{sat}^{L}(p) - u_{min}} - 1 \quad (u_{min} \le u \le u_{sat}^{L}(p)) \tag{4.25}$$

In two phase, the normalized internal energy is defined as eqation (4.27)

The normalized internal energy is equivalent to vapor quality.

$$\bar{u} = \frac{u - u_{sat}^{L}(p)}{u_{sat}^{V}(p) - u_{sat}^{L}(p)} \quad (u_{sat}^{L}(p) \le u \le u_{sat}^{V}(p)) \tag{4.26}$$

In superheated vapor phase, the normalized internal energy is defined as follows.

$$\bar{u} = \frac{u - u_{max}}{u_{max} - u_{sat}^{V}(p)} + 2 \quad (u_{sat}^{V}(p) \le u \le u_{max}) \tag{4.27}$$

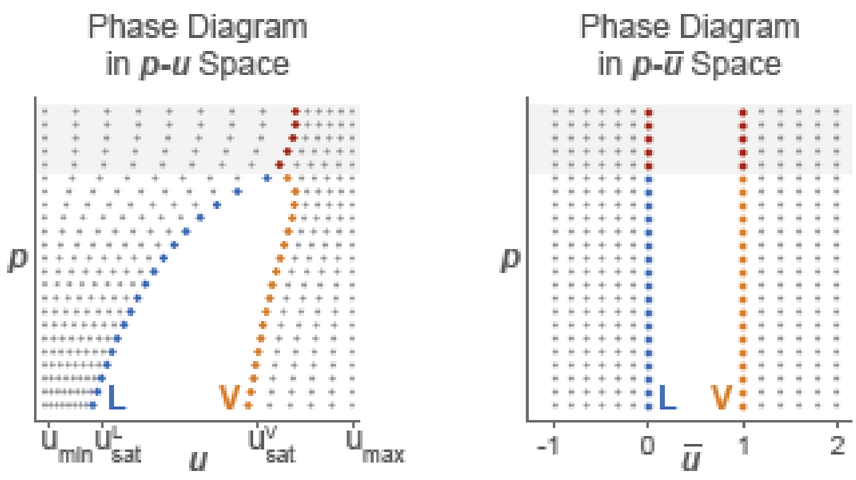

Fig.4.7 P-u diagram and P-$\bar{u}$ diagram [17]

In this study, the R32 property table is generated using the following code.

```
R32PropertyTables=twoPhaseFluidTables([100,580],[0.1,5],500,500,500,...'R32','C:¥Program Files (x86)¥REFPROP')
```

The code generates the table that range is 0.1 – 5 MPa pressure and 100 – 580 kJ/kg internal energy. The pressure and internal energy are divide into 500 segments.

The saturation temperature of refrigerant at evaporator and condenser outlet is calculated by edited block based on the "Thermodynamic Properties Sensor(2P)" block that calculate properties at connected point. The sensor block that calculate saturation temperature is created using "Simscape component" block and the edited source code of "Thermodynamic Properties Sensor(2P)". The superheat and subcool is calculated as follows.

$$Supereat = T_{Ref,Evap,out} - T_{sat,vap} = T_{Ref,Evap,out} - T(P_{Evap,out}, \bar{u} = 1) \tag{4.28}$$

$$Subcool = T_{sat,vap} - T_{Ref,Cond,out} = T(P_{Evap,out}, \bar{u} = 0) - T_{Ref,Cond,out} \tag{4.29}$$

4.1.6. Control system

The superheat, heat load, and heat sink/source outlet temperature is controlled with PI control system in the Simscape. Fig. 4.10 (a), (b), (c) show the control systems of them. The expansion valve opening area, compressor frequency, and heat sink/source volumetric flow rate are controlled based on the difference from the target value. In section 4.2, superheat is controlled by PI control (a), but compressor frequency and heat sink/source volumetric flow rate are defined as experimental values to compare with the experimental results. In section 4.4, compressor frequency and heat source volumetric flow rate are also controlled to compare the trends of cycle characteristics in the same condition.

Table 4.4 Parameters of P and I

Control of superheat	
P: 1×10^{-5}	I: 1×10^{-4}
Control of compressor frequency	
P: 10	I: 1×10^{-2}
Control of heat sink/source volumetric flow rate	
P: 1×10^{-8}	I: 1×10^{-8}

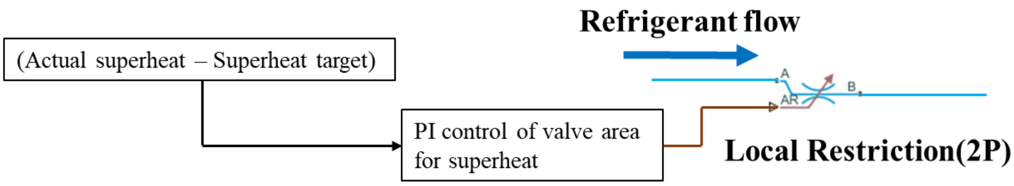

(a) PI control of expansion valve

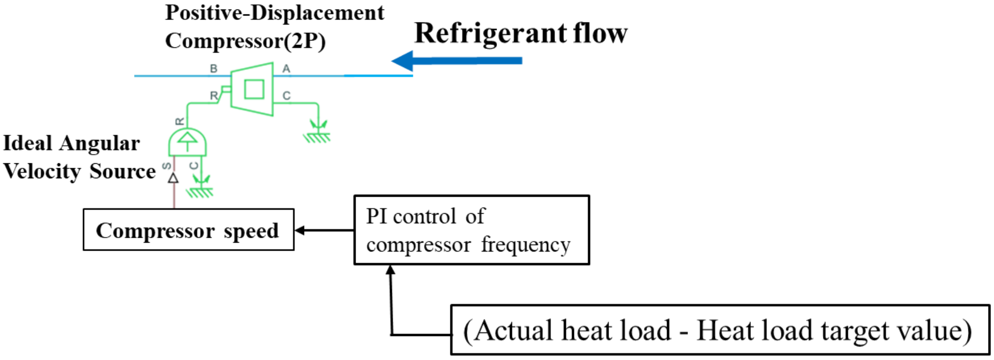

(b) PI control of compressor frequency

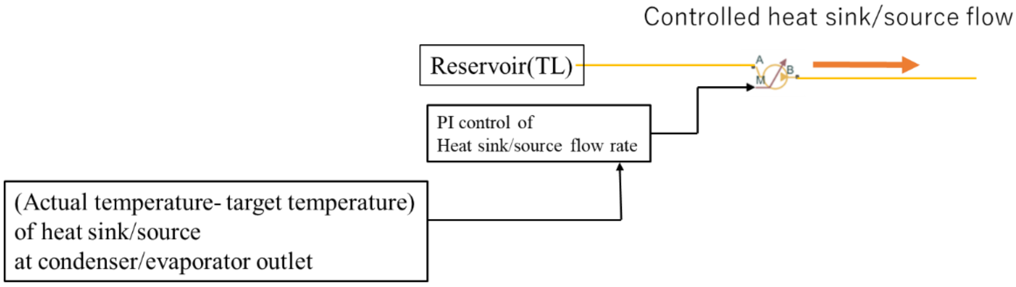

(c) PI control of heat source/sink flow rate

Fig. 4.8 PI control model

4.2. Comparison in Cooling condition

4.2.1. Heat exchange amount, refrigerant mass flow rate, compressor work, COP

Fig.4.9 shows the comparison of experimental results and simulative results in cooling condition. In the 2.2kW point, the simulation is not conducted because some error happened in the simulation. In all of the heat exchange amount, refrigerant mass flow rate, and compressor work, the prediction error is within 7%. However, the cooling COP in the simulation slightly increases as the heat load increases although the cooling COP in experimental results decreases. To discuss the trend of COP, the compressor work related to the condensation and evaporation pressure, and the degree of subcool should be considered.

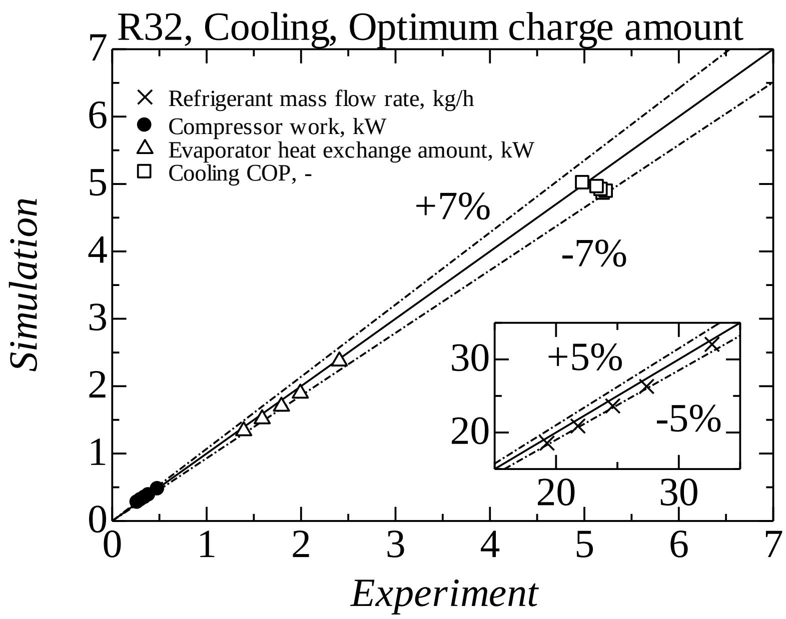

Fig. 4.9 Comparison of results in Cooling condition

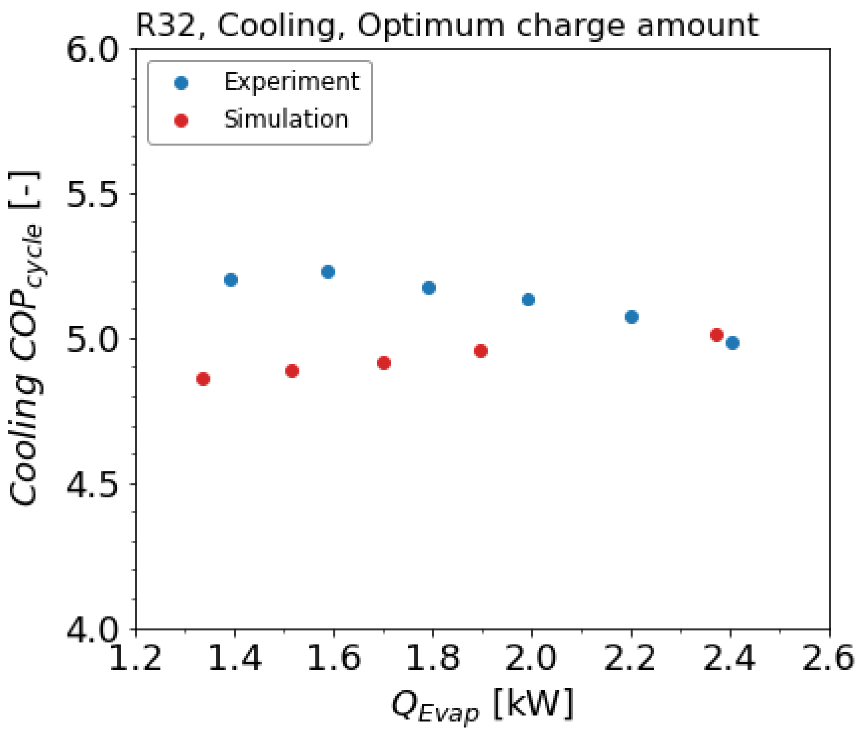

(a) Cooling cycle COP

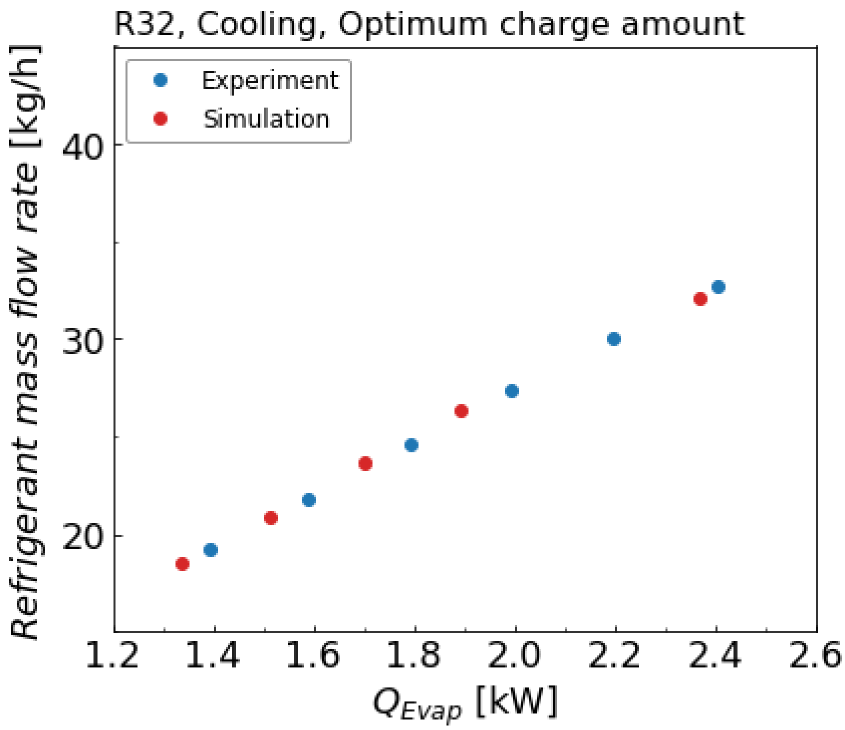

(b) Refrigerant mass flow rate

Fig. 4.10 Comparison of COP and mass flow rate

4.2.2. Pressure ratio and subcool

Fig. 4.13 shows comparison of the compressor pressure ratio and subcool. In the simulation, the accumulator set volume increases as heat load increases to reproduce the compressor pressure ratio. In low heat load, the compressor pressure ration in the simulation is high and subcool is low. Fig. 4.14 (a), (b) show the P-h diagram in 1.4kW and 2.4kW. In both of them, the condensation and evaporation pressure is different between experiment and simulation. The compressor pressure ratio can be increased by increasing accumulator volume. But in 1.4kW, condensation pressure is higher and evaporation pressure is lower than experimental results. This means the heat transfer coefficient is predicted lower than the actual case and causes increasing pressure ratio. In the simulation, the heat exchanger length is 1.5 times longer considering the enhancement of heat transfer by the micro-fin tube, but results show the enhancement by the micro-fin tube is higher than the heat transfer correlation and compensation of heat exchanger length. This is because the heat transfer coefficient correlation is for condensation and only consider the convective flow. In evaporation, nucleate boiling also should be considered. If the evaporation heat transfer coefficient correlation that have nucleate boiling term is used, the evaporation pressure and pressure ratio will be close to experimental results.

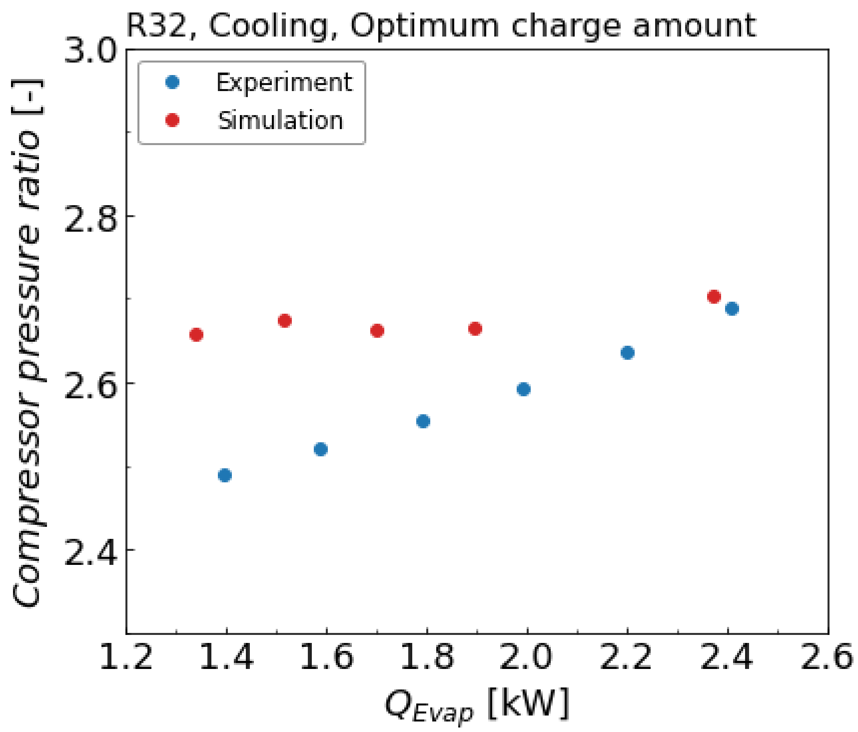

(a) Compressor pressure ratio

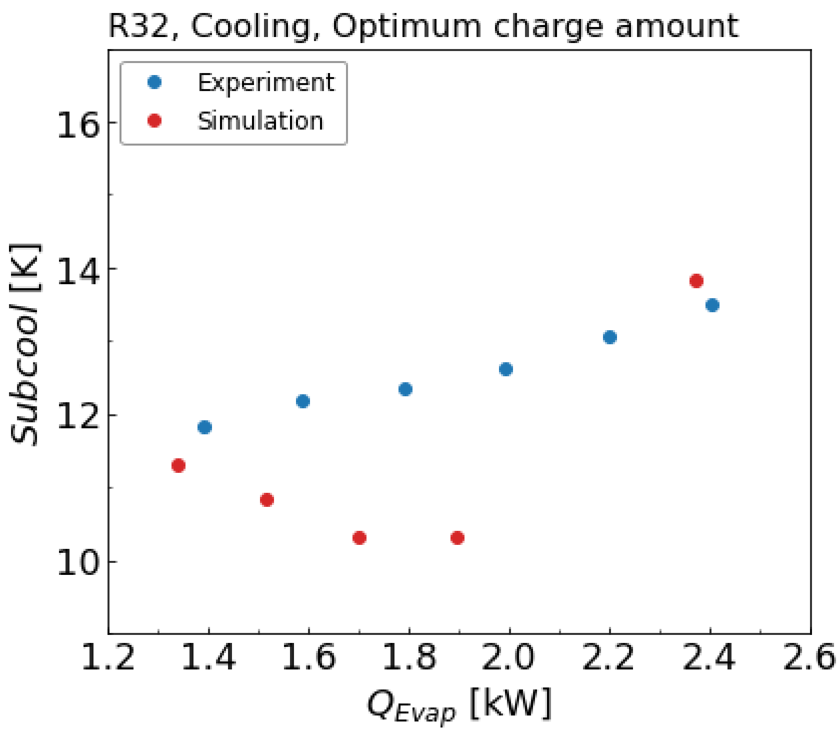

(b) Subcool

Fig.4.11 Comparison of pressure ratio and subcool

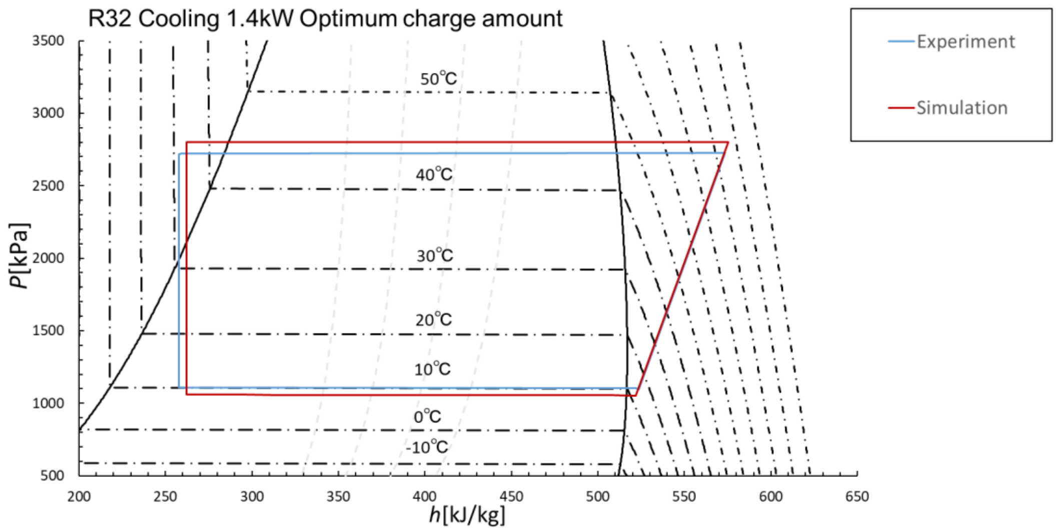

(a) Cooling 1.4kW

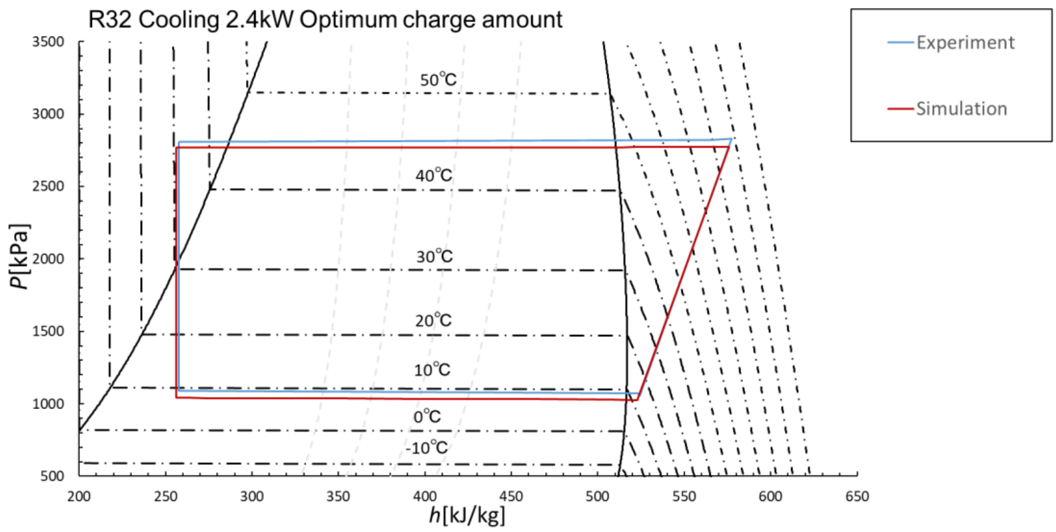

(b) Cooling 2.4kW

Fig. 4.12 Comparison of experiment and simulation on P-h diagram

4.3. Comparison in Heating and Low-load Heating condition

Fig. 4.15 (a), (b) shows the comparison of refrigerant mass flow rate, compressor work, heat exchange amount of condenser side, and heating COP. In heating condition, the prediction error is within 6% and the prediction error is within 8% in Low-load heating condition. However, the evaporation pressure is lower and condensation pressure is higher than experimental results condition, especially Low-load heating condition and it causes COP and pressure ratio trends to be significantly different from experimental results.

In all conditions, the refrigerant mass flow rate, compressor work, heat exchange amount, and COP are predicted with small error, 8%. But the more appropriate heat transfer coefficient correlation should be used to capture trends in change with increasing heat load and to improve accuracy without the correction of heat exchange length.

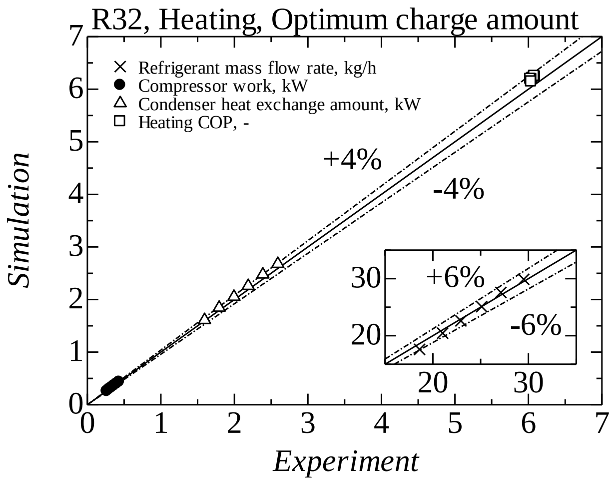

(a) Heating condition

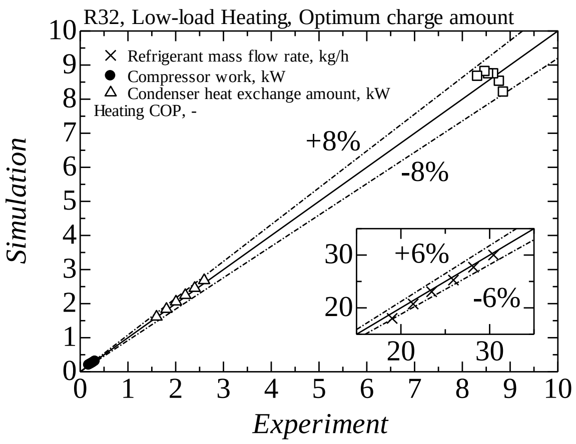

(b) Low-load Heating condition

Fig. 4.13 Comparison results in Heating condition and Loa-load Heating condition

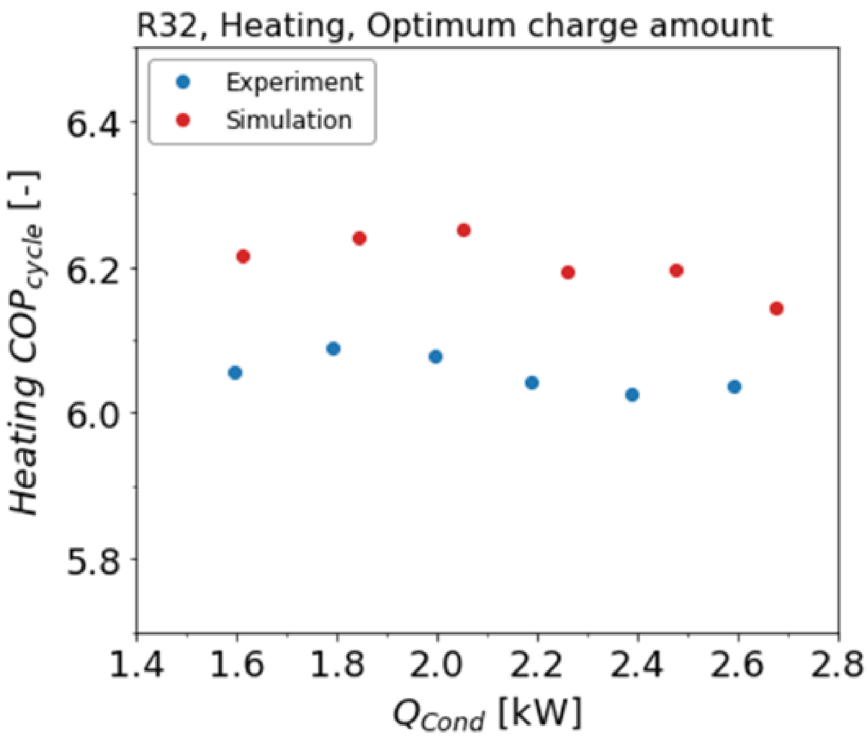

(a) Heating cycle COP

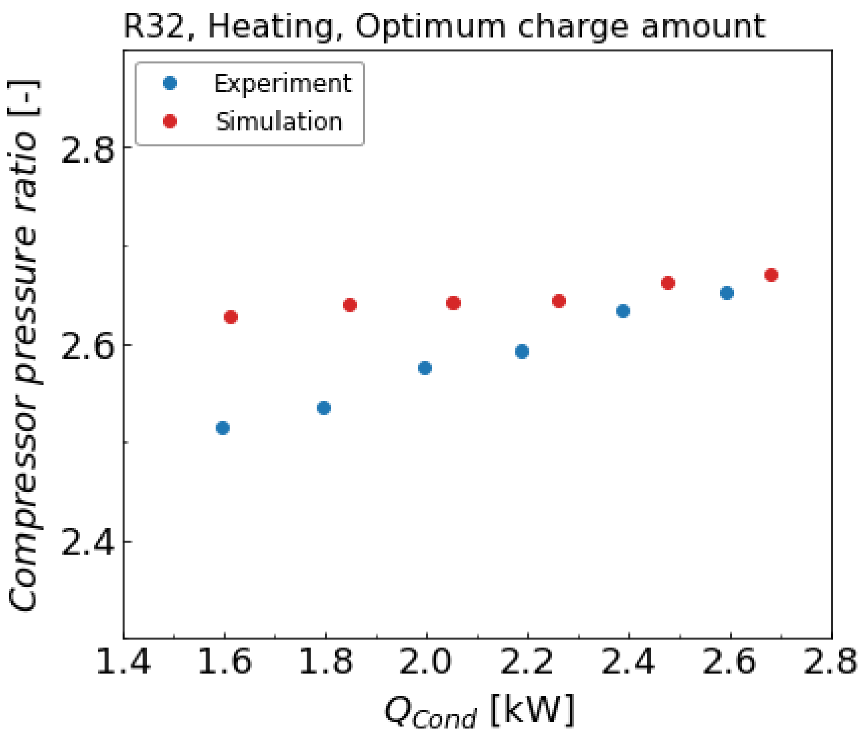

(b) Compressor pressure ratio

Fig. 4.14 Comparison of experiment and simulation (Heating condition)

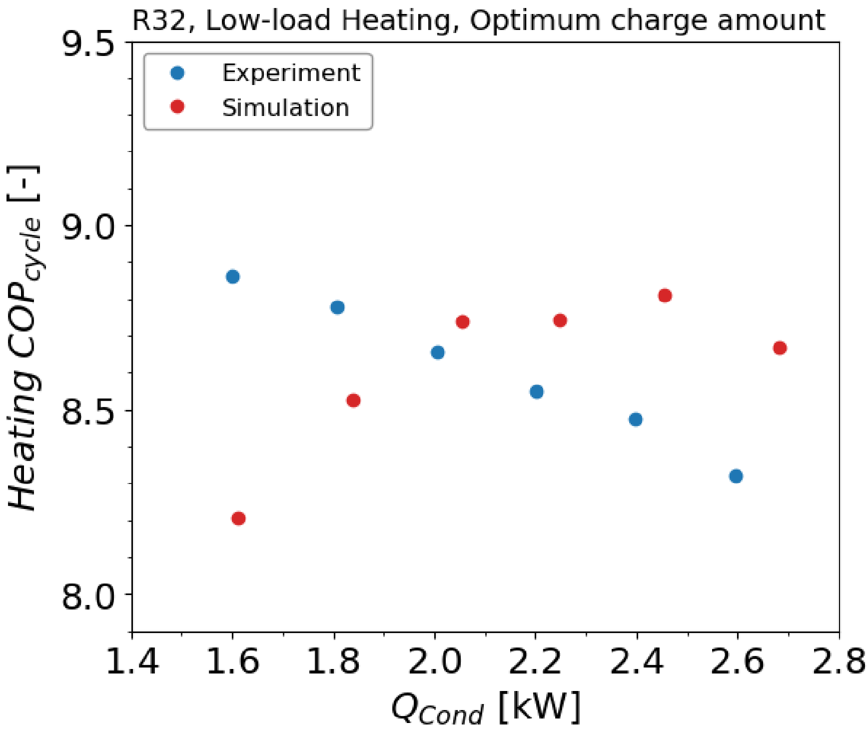

(a) Heating cycle COP

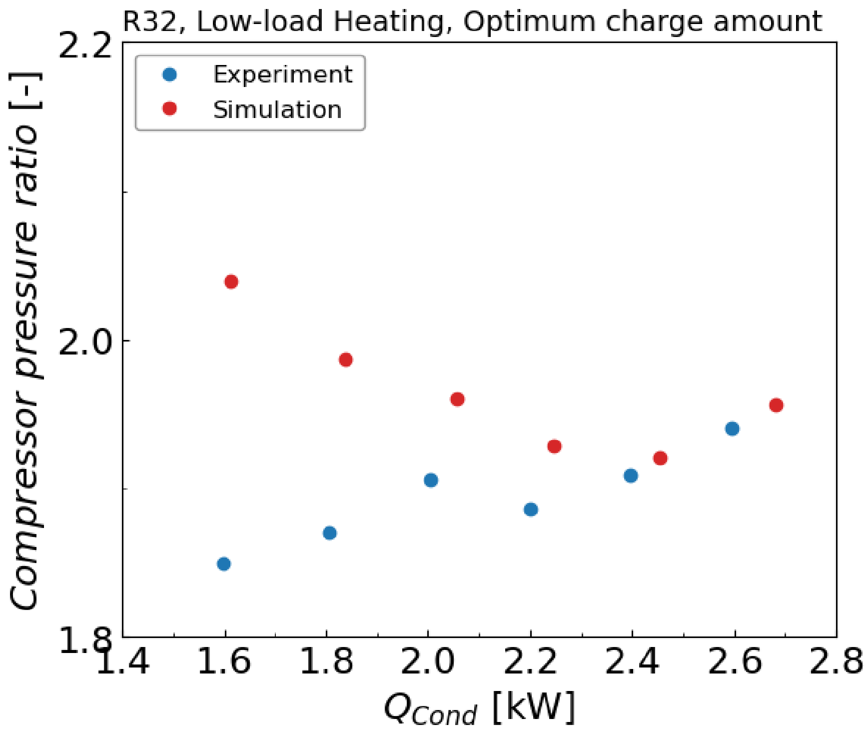

(b) Compressor pressure ratio

Fig. 4.15 Comparison of experiment and simulation (Low-load Heating condition)

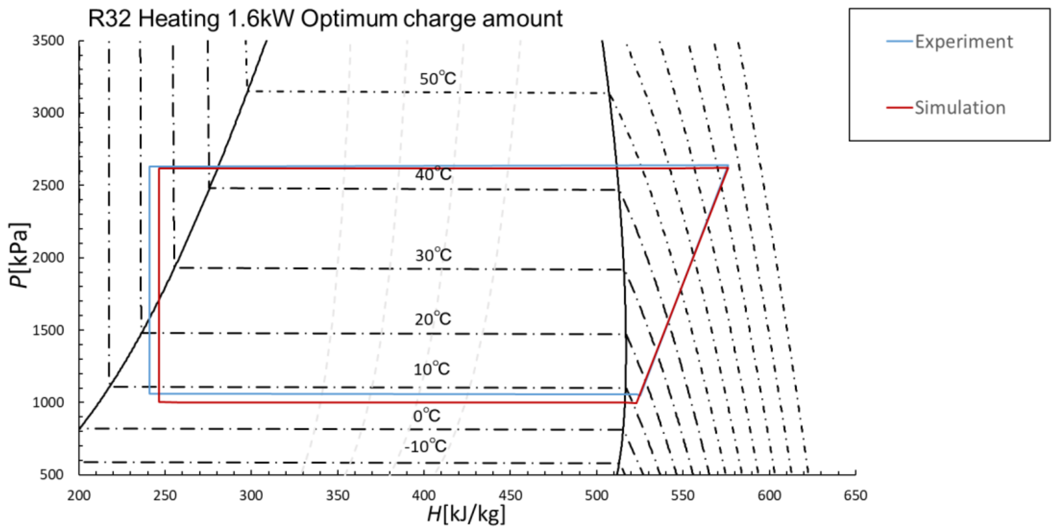

(a) Heating 1.6kW

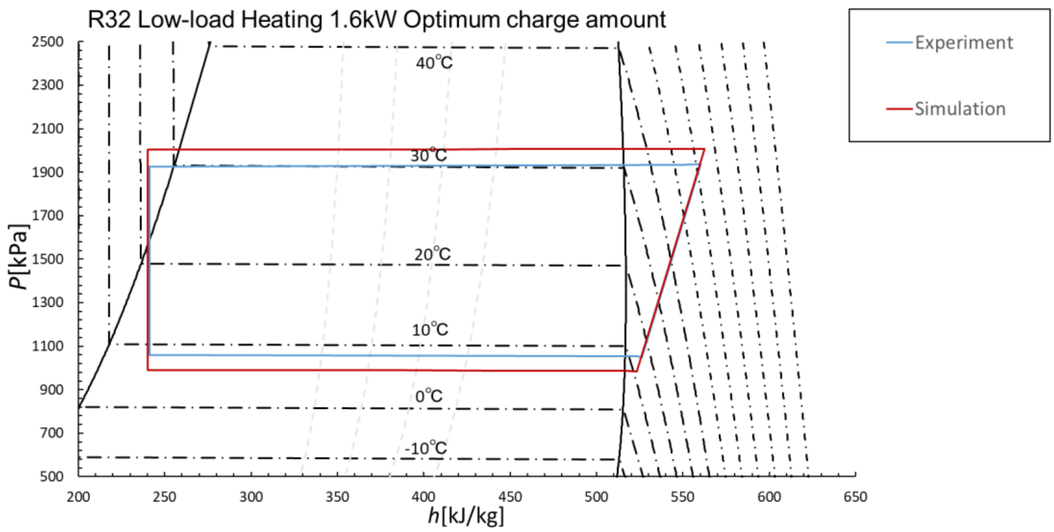

(b) Low-load Heating 1.6kW

Fig. 4.16 Comparison of experiment and simulation on P-h diagram

4.4. Reproduction of COP change in refrigerant charge amount

The performance of the heat pump also depends on the refrigerant charge amount. Takezato and Kawagita compared the cycle performance of the refrigerant using the optimum charge amount, the charge amount COP becomes highest.

The mechanism that optimum charge amount happens is as follows.

① As refrigerant charge amount increases, the subcooled liquid increases at the condenser outlet and the area fraction of vapor and two-phase decreases. The condensation pressure increases to enlarge temperature difference between refrigerant and heat sink and complete the condensation with decreased vapor and two-phase area.

② On the other hand, the area of subcooled liquid increases and subcooled liquid exchange more heat with the heat sink. That causes increasing subcool and decreasing pinch point. For constant heat exchange amount, refrigerant mass flow rate decreases since the enthalpy difference of refrigerant increases. However, the refrigerant heat transfer coefficient decreases as refrigerant mass flow rate decreases, so the cycle is stable at the point that increasing temperature difference between refrigerant and heat sink and decreasing refrigerant heat transfer coefficient for same heat exchange amount. At the point, the COP is improved since the refrigerant enthalpy difference increases and refrigerant mass flow rate decreases although the condensation pressure increases.

③ However, the subcooled liquid cannot exchange more heat after pinch point is zero, meaning refrigerant outlet temperature reaches heat sink inlet point. But condensation pressure increases as charge amount increases because of ①. To get enough enthalpy difference, the condensation pressure should be higher to increase the enthalpy at compressor discharge. Therefore, the compressor work and compressor pressure ratio increase significantly from the charge amount that pinch point is zero and finally contributes to decreasing COP.

In Simscape heat pump mode, this mechanism is reproduced by controlling accumulator volume. The refrigerant mass flow rate decreases as accumulator volume increases since the refrigerant stores in the tank. That contributes to increasing compressor pressure ratio to increase the temperature difference between the refrigerant and the heat sink.

In this section, the simulative results when accumulator volume increases are compared with the experimental results when refrigerant charge amount increases in Heating 1.6kW. In the simulation, the compressor frequency and heat sink/ flow rate are controlled by PI control (b) and (c) in section

4.4 for setting the heat load and heat sink/source outlet temperature to the condition to compare the trends of subcool, compressor pressure ratio, refrigerant mass flow rate, and COP.

Fig. 4.21 shows the pressure ratio of experimental and simulative results respectively. Although the pressure ratio in the simulation is higher than that of the experiment because of the accuracy of the heat transfer model, the pressure ratio of the simulation increases as accumulator volume increases. Fig. 4. Shows the P-h diagram of the simulative results. As accumulator volume increases, the condensation pressure and subcool increases. After refrigerant temperature at condenser outlet reaches the heat sink inlet temperature, the condensation pressure increases significantly. Fig. 4.23 and Fig.4.24 shows the comparison of refrigerant mass flow rate and the heating COP. The simulation reproduces the trend that refrigerant mass flow rate decreases and COP start to decrease around subcool 20K.

It is predicted that the other components such as connecting pipe should be modeled to reproduce the refrigerant charge amount, but the heat pump model will become more complicated. By using the accumulator volume, the trends of the cycle characteristics according to the refrigerant charge amount can be reproduced If the more sophisticated heat transfer model is used, the COP trends and the highest COP can be simulated. This will help select the optimum refrigerant in terms of the performances.

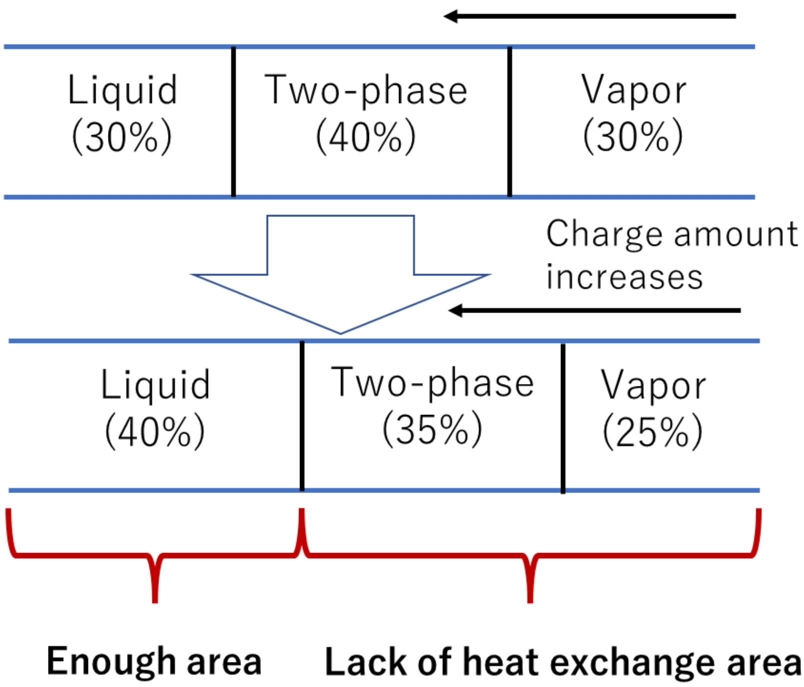

Fig. 4.17 Images of area fraction of refrigerant in condenser (Percentage is example)

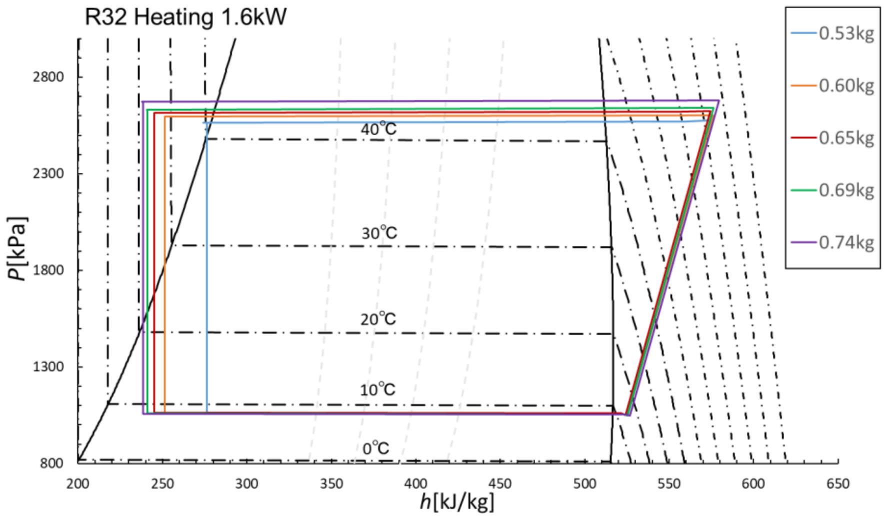

Fig. 4.18 P-h diagram of experimental results (Heating, 1.6kW)

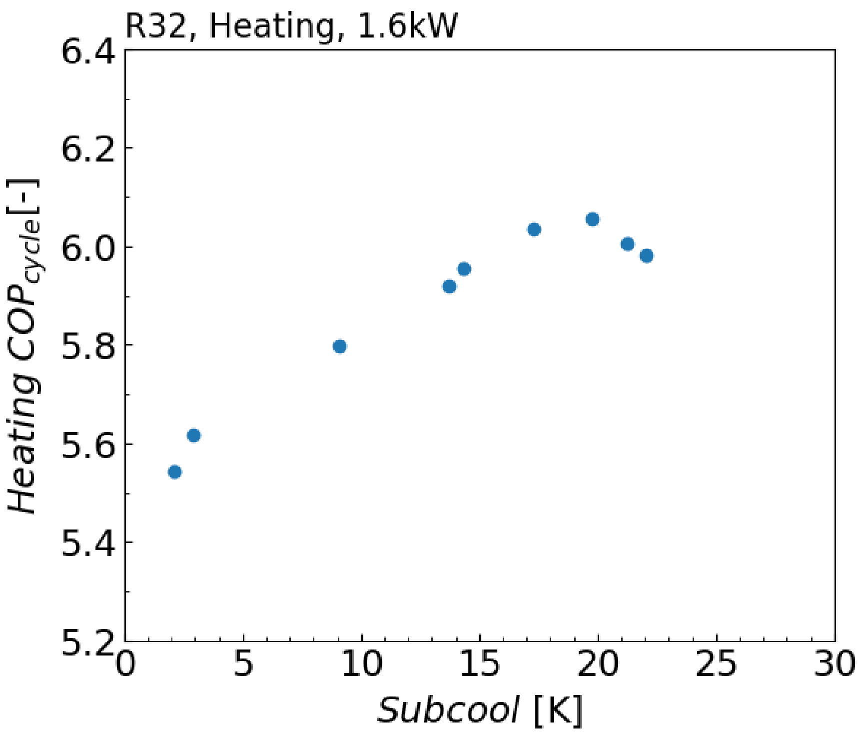

Fig. 4.19 COP and Subcool of experimental results

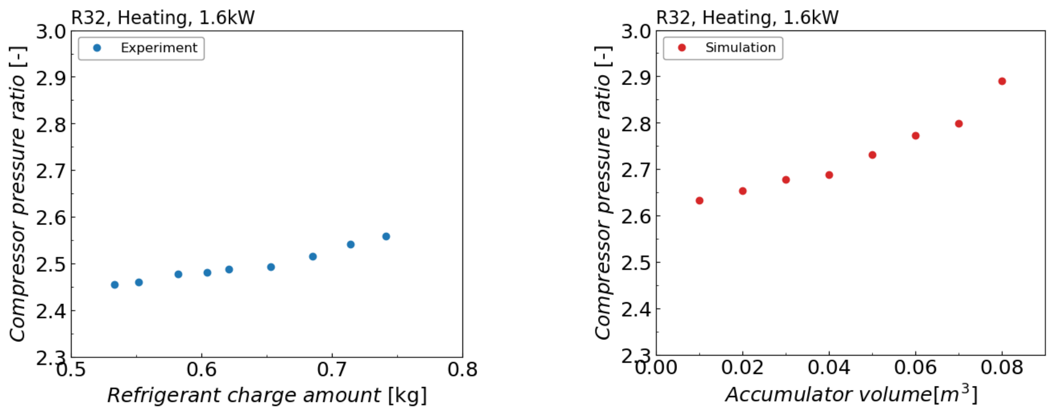

Fig. 4.20 Comparison of the trend of compressor pressure ratio

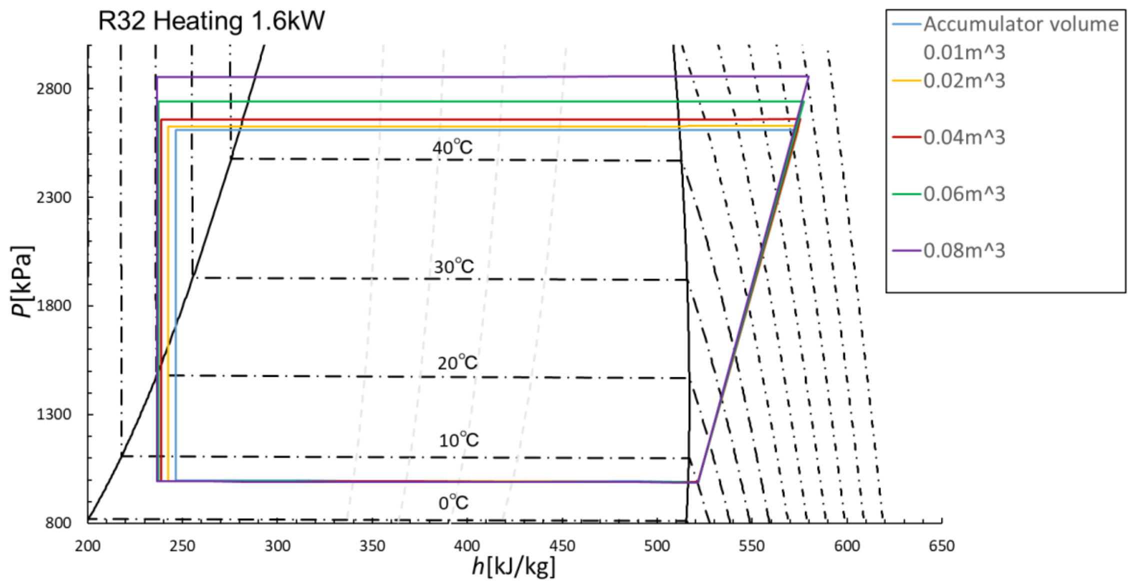

Fig. 4.21 P-h diagram of simulative results (Heating, 1.6kW)

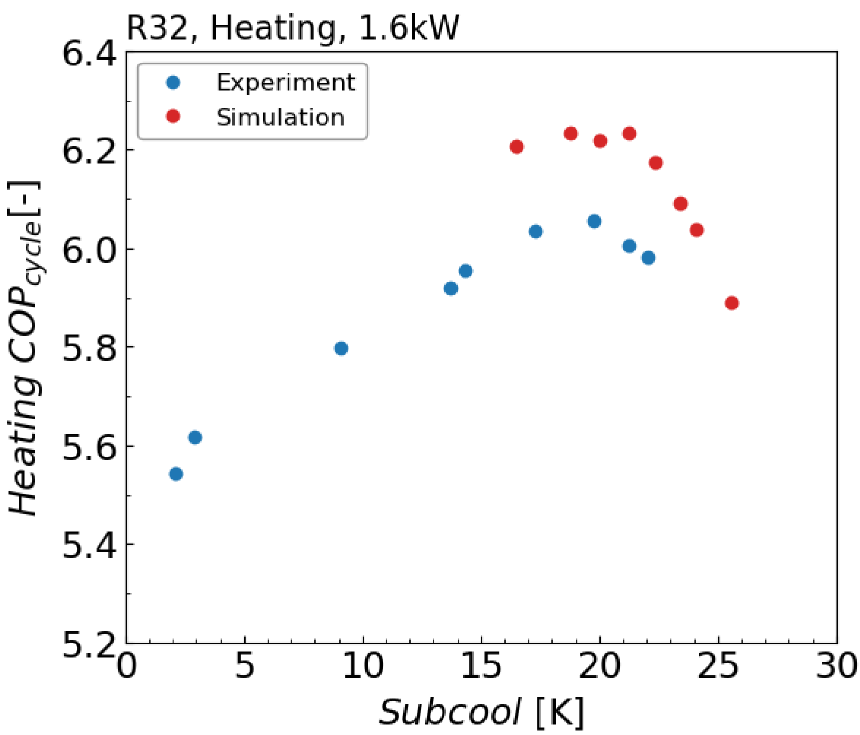

Fig. 4.22 Heating cycle COP (Heating, 1.6kW)

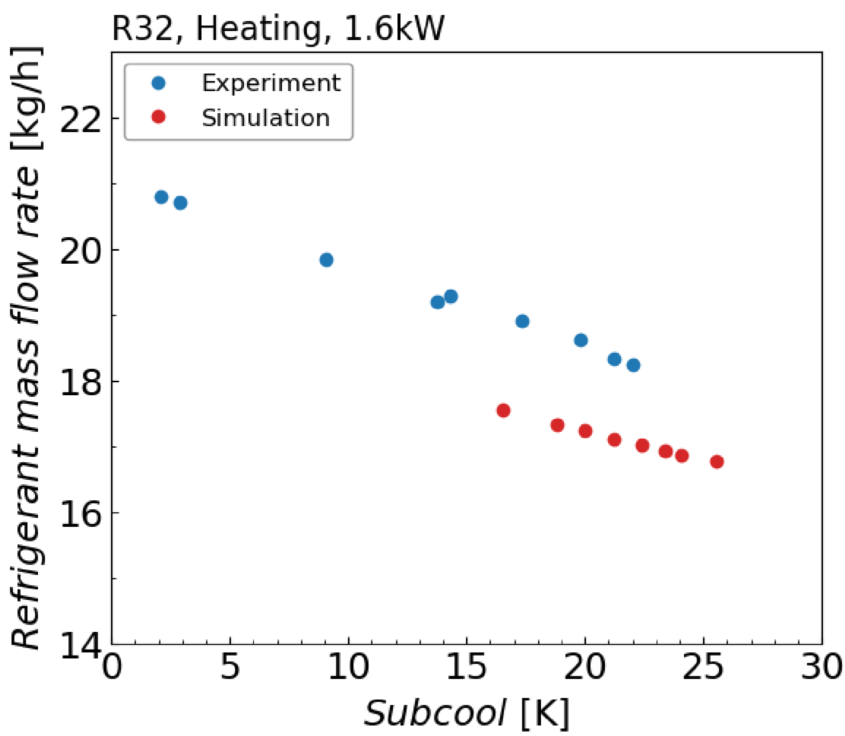

Fig. 4.23 Refrigerant mass flow rate (Heating, 1.6kW)

4.5. Challenges in heat pump modeling on Simscape

4.5.1. Restriction of heat transfer coefficient correlation

In the comparison of experiment and simulation, evaporation and condensation pressure, heat exchange amount, and COP are different. To improve the prediction accuracy, more appropriate correlation for evaporation and condensation heat transfer should be introduced. The Cavallini and Zecchin correlation is relatively simple correlation based on the Dittus-Boelter correlation, so other correlations considering enhancement of heat transfer by micro-fin tube such as Cavallini(1999) correlation for evaporation heat transfer will be appropriate. But some of the correlations are complicated and causes problems in Simscape.

The first one is variety of the fluid property. Table4. shows properties in the fluid property table. The surface tension is not in the table, so it is necessary to introduce the correlation according to the refrigerant. Equation (4. 30) is the empirical correlation for R32 surface tension[18].

$$\sigma = 71.47\left(1 - \frac{T}{351.26}\right)^{1.246} \tag{4.30}$$

To use the heat transfer correlation that include the surface tension, the surface tension correlation should be introduced to the "Pipe(2P)" block. If the cross area of the heat exchanger is big, the effect of surface tension will be small, and it is not necessary to use the heat transfer coefficient correlation that include the surface tension.

The second challenge is introduction of correlations of heat transfer coefficient and pressure drop. Various correlations are suggested according to refrigerant and type of heat exchanger. To improve prediction accuracy, appropriate correlation should be installed. Some of the heat transfer coefficient correlations include heat flux to consider the nucleate boiling. But the heat flux is derived from heat exchange amount, that is calculated using the heat transfer coefficient. That causes non-converging of the solver calculation in Simscape. If convective boiling is dominant and heat flux is not included in heat transfer coefficient correlation, the correlation can be used in the Simscape. In pressure drop, Darcy-Weisbach Equation and Haaland friction factor is used for both of single-phase and two-phase. When the pressure drop correlation for R32 in microfin-tube is introduced, the simulation became unstable. In the developed model, Solution does not converge in the early stages of simulation due to compatibility issues with the Receiver block at condenser outlet. If the model becomes more complex like introduction of the heat pump to existing systems, similar problems can be happened

Table 4.5 Available fluid property on Simscape

Pressure P	Internal energy u (⇒Normalized internal energy $\bar{u}$
Temperature T	Entropy s
Specific volume v	Thermal conductivity λ
Kinematic viscosity η	Prandtl number *Pr*
Calculable Properties	
Density ρ $(=\frac{1}{v})$	Viscosityμ $(=\eta * \rho)$
Constant pressure specific heat $c_p = \frac{Pr * \lambda}{\mu}$	
Property not in the property table	
Surface tension σ	

4.5.2. Property of refrigerant mixture in Simscape

As explained in section 4.1.5, the property of the fluid is calculated using the P-$\bar{u}$ table. The property table of the various refrigerant can be created via REFPROP including the registered refrigerant mixture such as R410A and defined mixtures such as R32/R1234yf/CO_2 (22/72/6 mass%).

In this section, the property of the refrigerant mixture is compared with the REFPROP Ver. 10.0. Fig. 4.24 shows the comparison of MATLAB property table and REFPROP on P-h diagram and T-s diagram. The saturation liquid and vapor line of MATLAB property table is made using the property data where the normalized internal energy is 0 and 1 in the matrix. In the T-s diagram, the points of the MATLAB property table is compared with the temperature and entropy derived from pressure and enthalpy in REFPROP. The saturation point is not plot in T-s diagram since the points cannot be plot exactly. In refrigerant mixtures, the green line is the saturation line that the reference point is "Currently defined mixture" and the red line is the saturation line that the reference point is "Each pure components". As shown in Fig. 4.24 (b), (c), and (d), the reference point of the MATLAB property table is that of "Each pure components". However, the points in the two-phase refrigerant mixtures are different from the REFPROP "Currently defined mixture" value although the saturation line and points in single-phase is almost same as value of the REFPROP. This is because the two-phase is calculated using the interpolation of liquid and vapor phase in MATLAB property table. In comparison of temperature at evaporator inlet, the error increases as temperature glide increases in the zeotropic mixtures,

The Property table in MATLAB is reliable in pure fluid and the error is relatively small in azeotropic mixtures, but the property error in zeotropic mixtures cannot be negligible. The other properties in table 4.5 will be also different from the value in REFPROP and affect the calculation in heat exchange process including the calculation of heat transfer coefficient.

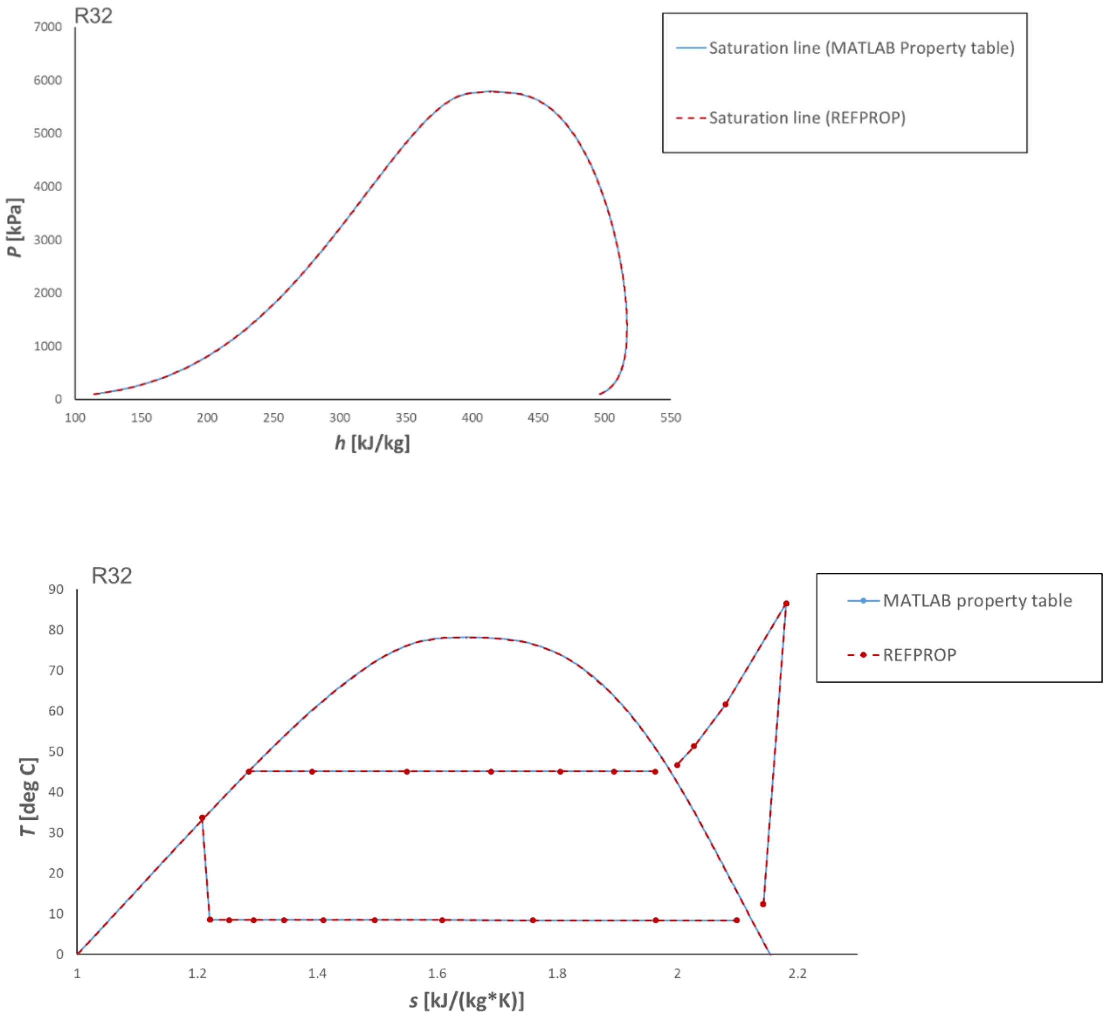
R32
P [kPa]
h [kJ/kg]
Saturation line (MATLAB Property table)
Saturation line (REFPROP)
R32
T [deg C]
s [kJ/(kg*K)]
MATLAB property table
REFPROP

(a) R32

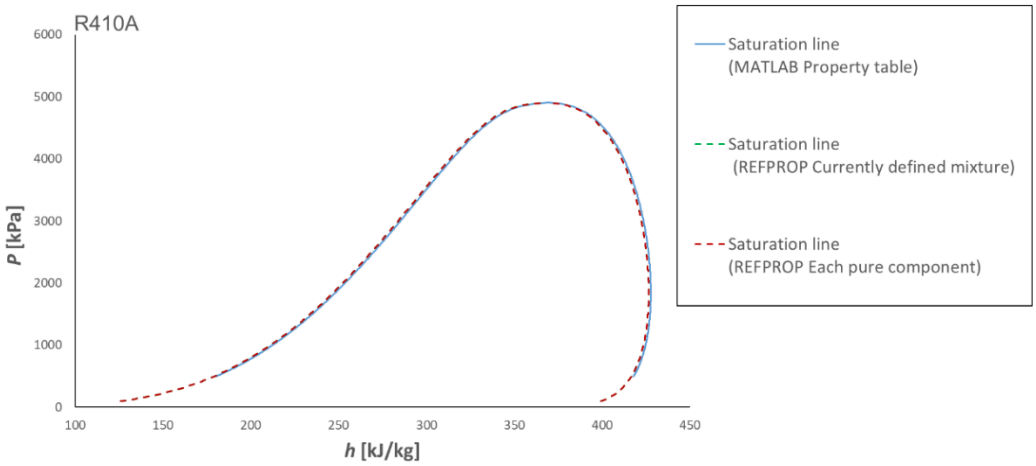
R410A
P [kPa]
h [kJ/kg]
Saturation line
(MATLAB Property table)
Saturation line
(REFPROP Currently defined mixture)
Saturation line
(REFPROP Each pure component)

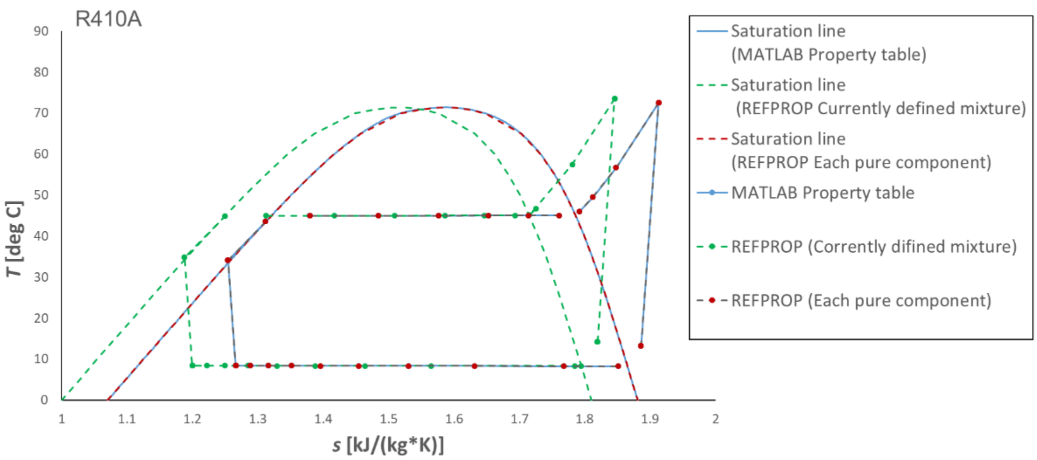

(b) R410A (R32/R125 50/50 mass%)

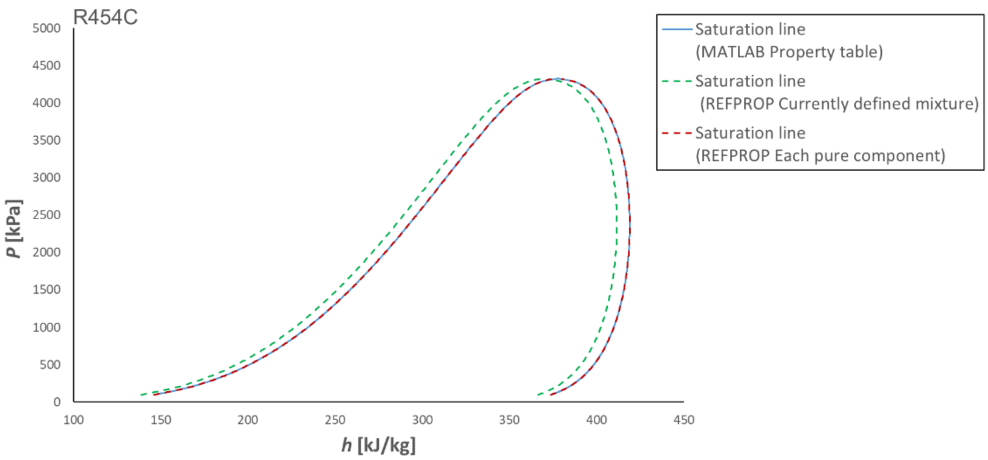

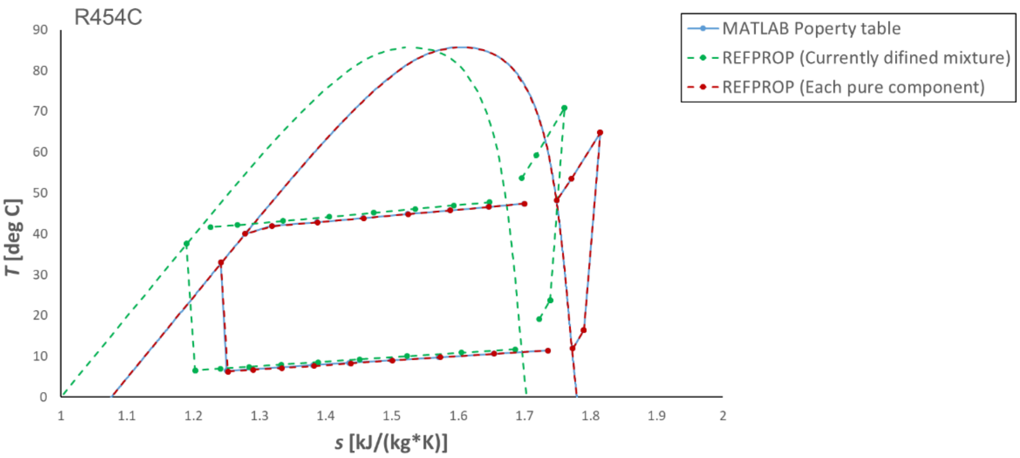

(c) R454C (R32/R1234yf 21.5/78.5 mass%)

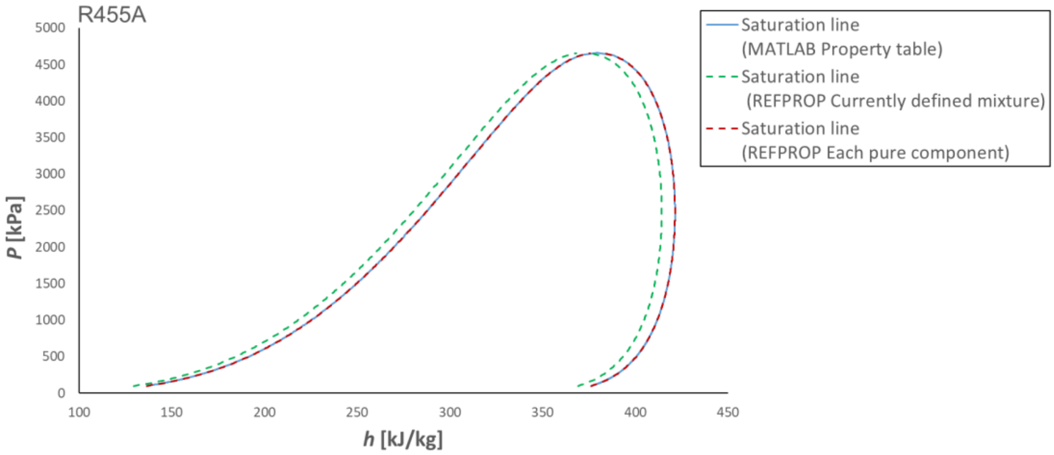

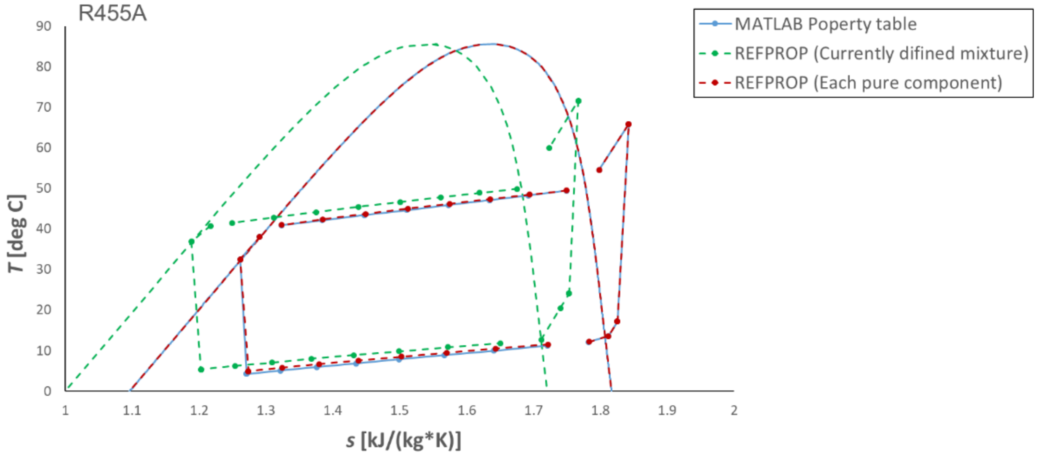

(d) R455A (R32/R1234yf/CO_2 21.5/75.5/3 mass%)

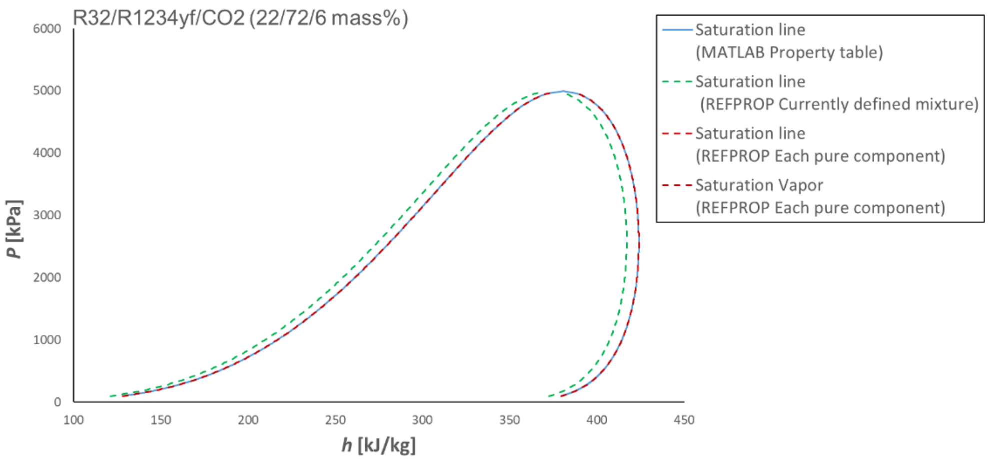

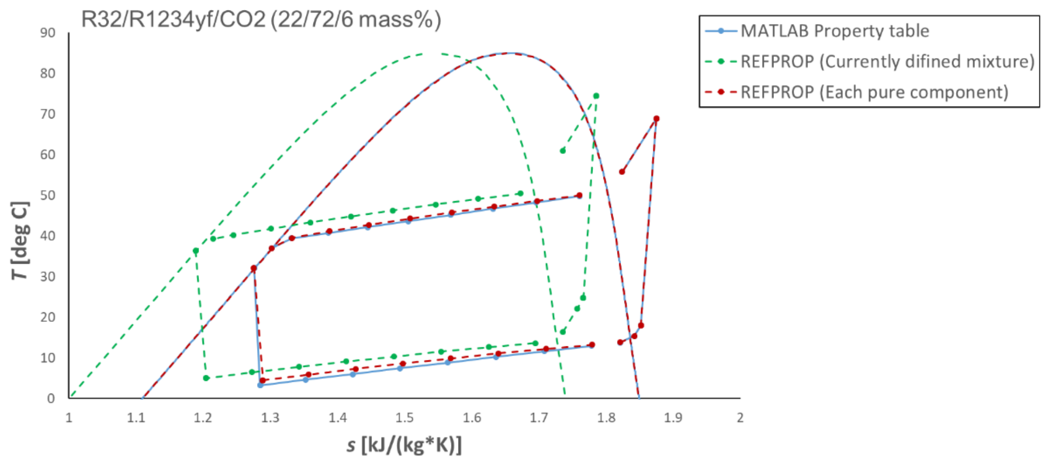

(e) R32/R1234yf/CO_2 (22/72/6 mass%)

Fig. 4.24 Comparison of property difference between MATLAB property table and REFPROP Ver. 10.0

Table 4.6 Temperature difference between MATLAB property table and REFPROP at evaporator inlet point

Refrigerant	Temperature glide* [K]	MATLAB Property table [℃]	REFPROP (Currently defined mixture) [℃]	Error [℃]
R32	-	8.5189	8.5189	-1.2933E-05
R410A	0 (Azeotropic)	8.4104	8.4078	0.0026
R454C	7.4	6.4836	6.2797	0.2039
R455A	11.0	4.2804	4.9355	-0.6551
R32/R1234yf/CO_2 (22/72/6 mass%)	14.2	3.2818	4.4819	-1.2001

*: Value at bulk temperature 20℃

5. Conclusion

In this thesis, development of vapor compression heat pump cycle model on MATLAB Simscape environment is conducted and the simulation results are compared with experimental results. The contents are summarized as follows.

(1). In condensation and evaporation, the heat transfer coefficient of zeotropic refrigerant mixture R32/R1234yf (22/78 mass%) and R32/R1234yf/CO_2 (22/74/4 mass%, 22/72/6 mass%) are lower than current azeotropic mixture R404A because of mass transfer resistance due to temperature glide.

(2). In both of condenser and evaporator side, the overall thermal conductance UA of zeotropic mixtures are predicted within 30% error. The Silver-Bell Ghaly correction and Shah correction for zeotropic mixture improve the correction accuracy.

(3). In R32, the Cavallini(2009) correlation and Cavallini and Zecchin correlation that is used in Simscape model do not predict the condensation heat transfer coefficient well in low refrigerant mass flow rate. The more accurate correlation or correction of heat exchanger length is necessary to improve the prediction accuracy of heat pump.

(4). The heat pump model including heat sink/source water flow is developed. The simulation model can be controlled with PI control system for target value of superheat, heat load, and heat sink/source water temperature at condenser and evaporator outlet. The control system enable to simulate heat pump cycle in various conditions

(5). In cooling, Heating, Low-load Heating conditions, the refrigerant mass flow rate, compressor work, heat exchange amount, and COP is predicted within 8% error. To improve the prediction accuracy, introduction of more accurate heat transfer coefficient correlation is necessary.

(6). The COP changes as refrigerant charge amount increases and there is COP highest point. This is caused by increasing subcooled liquid at condenser outlet and increasing condensation pressure. In the simulation, the influence of refrigerant charge amount to cycle characteristics is reproduced. This will help compare the COP of the refrigerants.

(7). It is necessary to import the surface tension equation for introducing various heat transfer coefficient correlations. And the reference point of the refrigerant mixture property table in MATLAB is that of each pure components. For analysis of the heat pump cycle of the alternative refrigerant mixtures, the correction for heat transfer coefficient correlation will improve the accuracy as mentioned in (2). But the correction includes the heat flux and make it difficult to converge solution in Simscape simulation. It is also confirmed that introduction of pressure drop correlation in single-phase and two-phase causes instability of the simulation.

The developed heat pump cycle model can simulate the cycle characteristics with high accuracy in pure refrigerant R32. In near future, the zeotropic refrigerant mixtures are options for alternatives. The correction for heat transfer coefficient will help improve the prediction accuracy.If the above challenges are solved, the developed heat pump model will be useful to evaluate the effect of heat pump installation and to determine the optimal environmentally friendly refrigerant for various fields.

Acknowledgement

The thesis is dedicated to Pusan National University as a part of the double degree program in the “Campus Asia Program” with a lot of cooperation. I would like to express my gratitude to all of those who contributed to my study.

I would like to express my deepest gratitude to Prof. Takahiko Miyazaki, Professor, Department of Advanced Environmental Science and Engineering, Faculty of Engineering Sciences, Kyushu University, for providing me with accurate and useful guidance and encouragement from the beginning to the details in carrying out my research. I also received a lot of guidance and encouragement while organizing this thesis.

I am sincerely grateful to Prof. Kyaw, Associate Professor, Department of Advanced Environmental Science and Engineering, Faculty of Engineering Sciences, Kyushu University, for providing invaluable guidance and enthusiastic support, which significantly contributed to the progress of my research. Furthermore, I am deeply thankful for his precise and considerate guidance on data analysis and addressing my inquiries.

I am grateful for the guidance and advice provided by Prof. Ji Hwan Jeong, Professor, School of Mechanical Engineering, Pusan National University, during my stay in Pusan National University. His support helped me proceed with my research and broaden my knowledge, especially about heat transfer.

I would like to express my deepest gratitude to Nobuo Takata, Technical Specialist, Department of Advanced Environmental Science and Engineering, Faculty of Engineering Sciences, Kyushu University, for providing me with guidance and encouragement in carrying out this research. I am also grateful for his assistance in conducting experiments safely and smoothly.

Mr. Kanta Kawagita, Mr. Taiki Arima, Mr. Norito Kudo helped me a lot in the experiment, simulation, preparation of materials, and discussions about the research until late at night. I would like to express my sincere appreciation.

Mrs. Yuri Yamato, the laboratory secretary, supported me with many administrative procedures. I am grateful for her help.

I would like to express my sincere appreciation to Prof. Wang Dong, Ms. Nahoko Ichimura, Ms. Chiaki Harasaki, Ms. Miwa Tsuruta, and the professors and staff of the Campus Asia program at Kyushu University, Prof. Lee Donggeun, Ms. Lea, and the professors and staff of Pusan National University I would also like to thank the professors and staff at Shanghai Jiao Tong University and Universiti Teknologi Malaysia for their support.”

I would like to express my appreciation to my laboratory members at Kyushu University and Pusan National University for their help.

Finally, I express my appreciation to my parents for their encouragement.

Reference

[1]. Office of Fluorocarbons Control Policy, Ministry of the Environment, Japan, Japan's Policies of fluorocarbons management (refrigerant transition) Fluoride Gases Management Office, Ministry of Economy, Trade and Industry, https://ozone.unep.org/system/files/documents/3_Japans%20Policies%20of%20Fluorocarbons%20management%20_refrigerant%20transition.pdf ,2019

[2]. 未利用熱エネルギー革新的活用技術研究組合　技術開発センター，産業分野の排熱実態調査報告書, https://www.nedo.go.jp/content/100957934.pdf, 2019

(Thermal Management Materials and Technology Research Association, Survey Report on Exhaust Heat from Factory Equipment in 15 Industries, (2019))

[3]. NEDO, Paving Way to Realize Energy Conservation and Carbon Neutrality Utilization Thermal Energy Technology, focus NEDO No.87, 2023

[4]. Fukuda Sho, Kojima Hideki, Kondou Chieko, Takata Nobuo, Koyama Shigeru, Comparative assessment on irreversible losses in heat pumps using R744/R32/R1234yf and R744/R32/R1234ze(E), Sci. Technil. Built Enviom. 22 (8) (2016), 1118-1127

[5]. Kyaw Thu，Kosei Takezato，Nobuo Takata，Takahiko Miyazaki，Yukihiro Higashi，“Performance evaluation of a heat pump system using an R-32/R-1234yf blend with GWP below 150 for heating applications”,Applid Thermal Engineering，Vol.182 (2021)

[6]. 川喜田幹太，2023，“冷蔵温度帯における低 GWP 混合冷媒ヒートポンプサイクルの実験および LCCP 評価”，修士論文，九州大学

(Kanta Kawagita, "Experimental and LCCP Evaluation of Low-GWP Mixed Refrigerant Heat Pump Cycles in the Refrigeration Temperature Range," Master's Thesis, Kyushu University.)

[7]. Kiyoshi Saito, Jongsoo Jeong, “Development of General Purpose Energy System Simulator”, Energy Procedia 14 (2012), 1595 – 1600

[8]. Singh, Shobhana; Sørensen, Kim, “Dynamic model of a heat pump based house heating system”, Proceedings of the 59th SIMS Conference on Simulation and Modelling, SIMS 2018

[9]. Jaedeok Ko, Nobuo Takata, Kyaw Thu, Takahiko Miyazaki， ” Dynamic Modeling and Validation of a Carbon Dioxide Heat Pump System”, Evergreen. 7 (2020), 172–194

[10]. E.W. Lemmon, M.L. Huber, M.O. McLinden, 2018. Reference Fluid Thermodynamic and Transport Properties - REFPROP Ver. 10.0. National Institute of Standards and Technology, Boulder, CO, USA.

[11]. E.W. Lemmon, M.L. Huber, M.O. McLinden, 2013. Reference Fluid Thermodynamic and Transport Properties - REFPROP Ver. 9.1. National Institute of Standards and Technology, Boulder, CO, USA.

[12]. Cavallini. A. Del Col, D. Doretti, L. Longo, G.A. Rossetto, L. “Refrigerant vapor-ization inside enhanced tubes: a heat transfer model”. Int. J. Heat Techonol. 17(2) (1999), 29-37

[13]. Cavallini. A., D. Del Col, S. Mancin, L. Rossetto, Condensation of pure and near-azeotropic refrigerants in microfin tubes: A new computational procedure, Int. J. Refrig 32 (2009),162–174,

[14]. C.H. Kim, N.H. Kim, Condensation heat transfer and pressure drop of low GWP R-404A-alternative refrigerants (R-448A, R-449A, R-455A, R-454C) in a 7.0-mm outer-diameter horizontal microfin tube, Int. J. Refrig. 128 (2021), 118–128

[15]. C.H. Kim, N.H. Kim, Evaporation heat transfer of the low GWP alternative refrigerants (R-448A, R-449A, R-455A, R-454C) for R-404A in a microfin tube, Int. J. Refrig. 128 (2021), 118–128

[16]. A. Cavallini, R. Zecchin, A dimensionless correlation for heat transfer in forced convection condensation. Proc. 6th Int. Heat Transf. Conf. vol. 3 (1974), pp. 309–313.

[17]. MathWorks®, “Two-Phase Fluid Properties (2P)”, 21 Oct. 2023

[18]. A. Mulero, I. Cachadiña, M.I.Parra, Recommended Correlations for the Surface Tension of Common Fluids, J. Phys. Chem. Ref. Data, Vol. 41, No. 4, 2012

Appendix A

Fig. A.1-A.6 show the components of the heat pump model on Simscape. The structure of the components is same as chapter 4, but the figures also include the sensor block to measure the fluid properties.

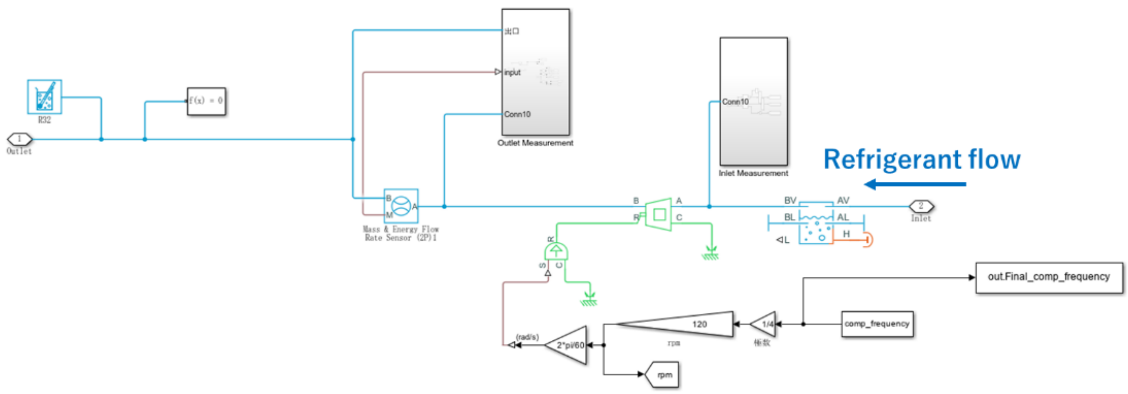

Fig. A.1 Compressor model

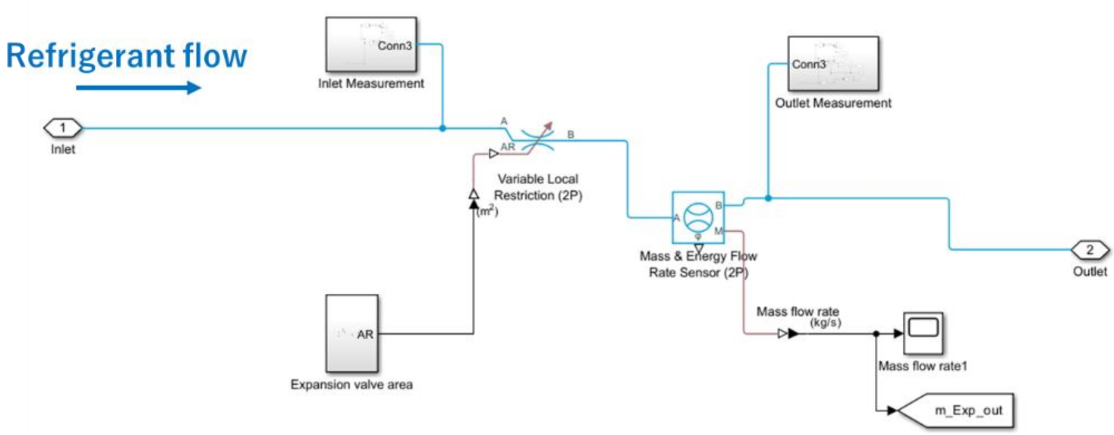

Fig. A.2 Expansion valve model

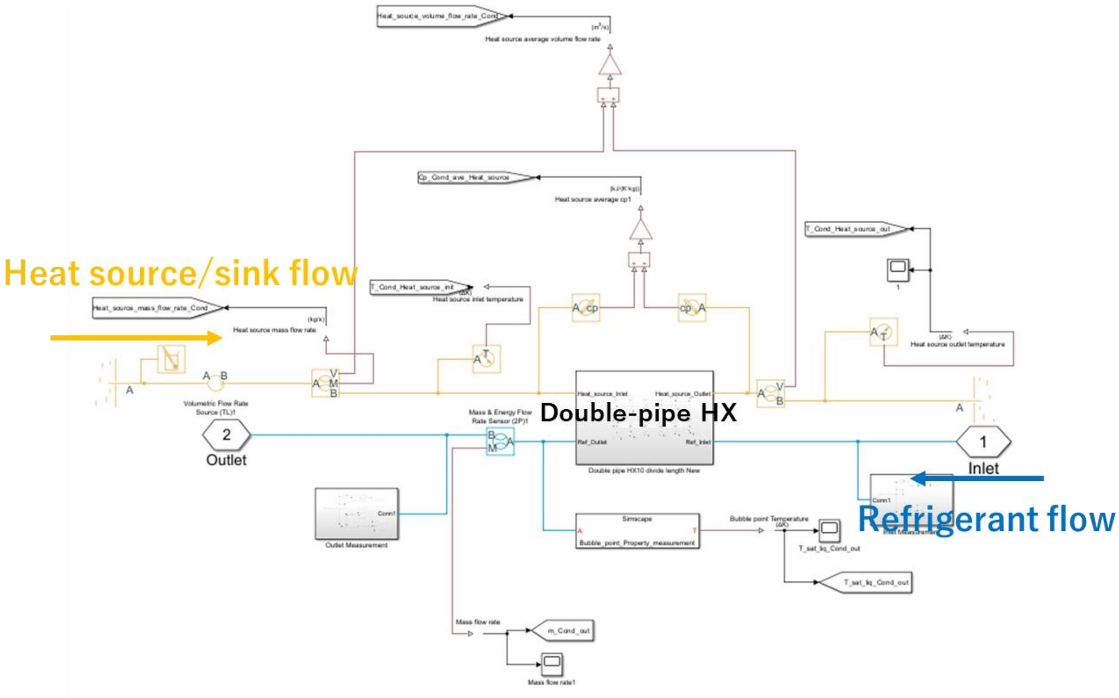

Fig. A.3 Model of refrigerant and heat sink/source flow in heat exchanger

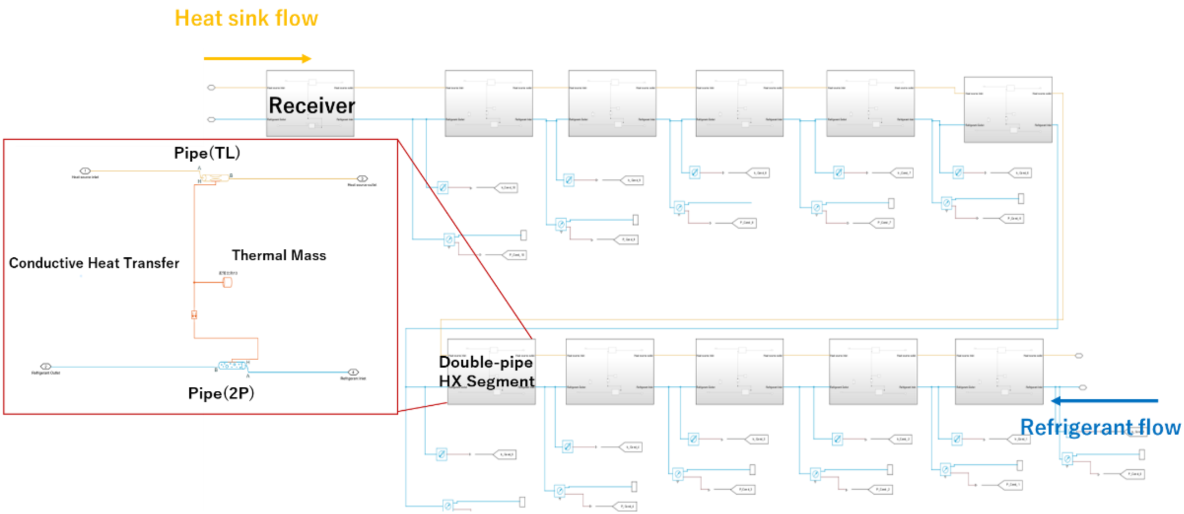

Fig. A.4 Condenser model

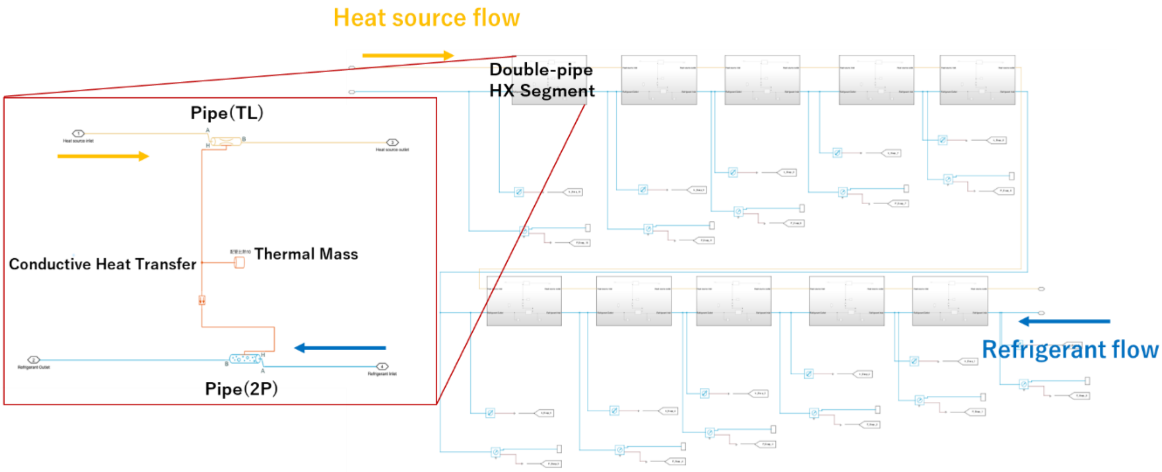

Fig. A.5 Evaporator model

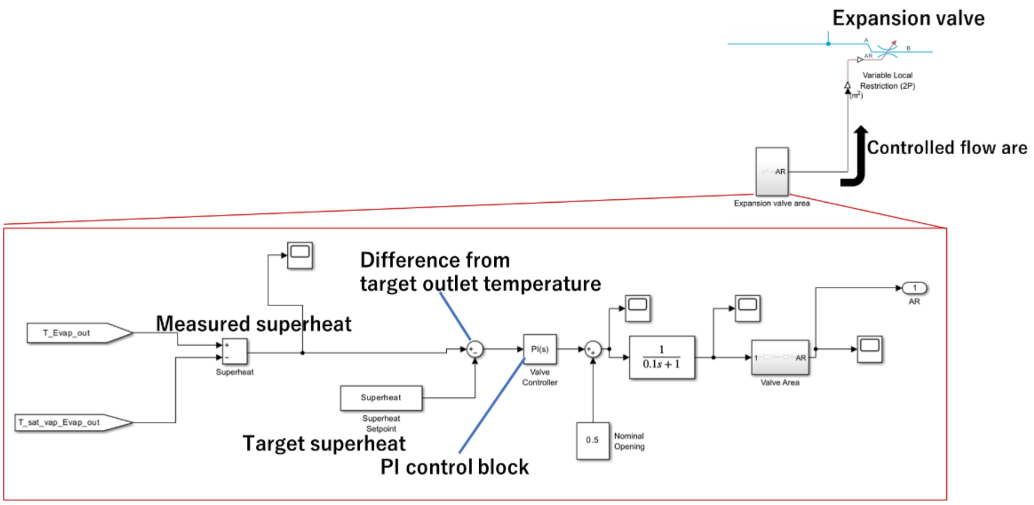

(a) Control of expansion valve opening for superheat

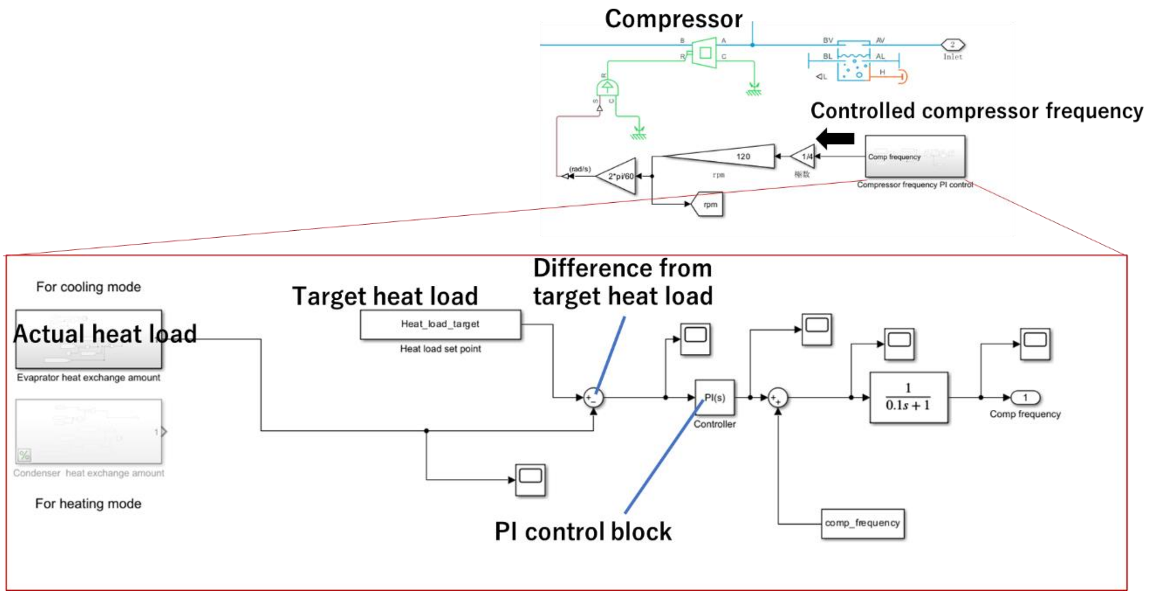

(b) Control of compressor frequency for heat load

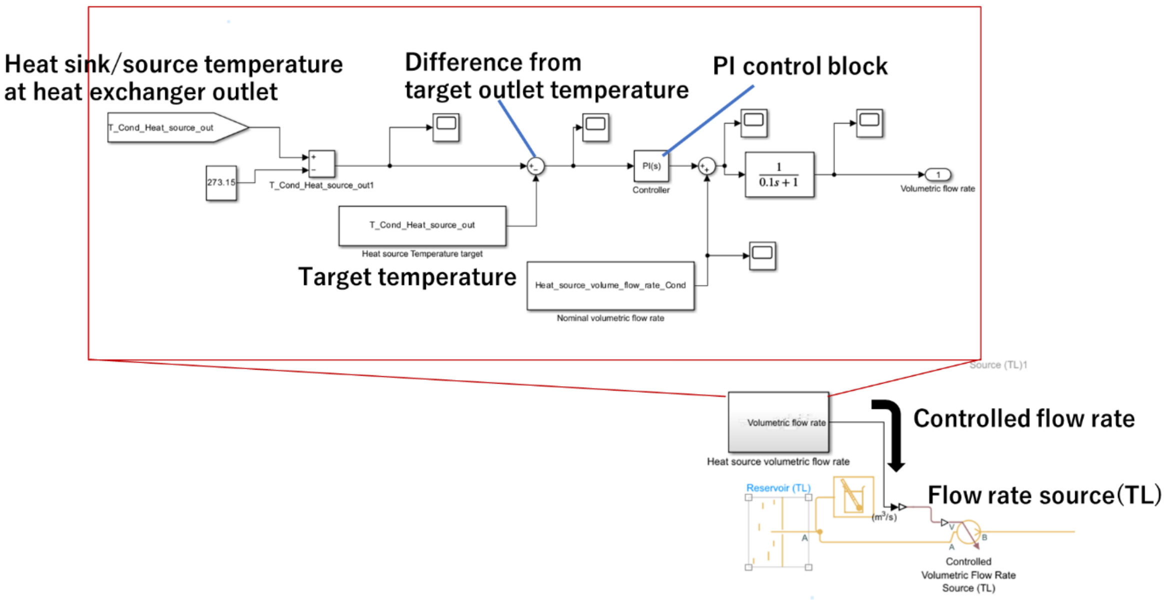

(c) Control of heat sink/source flow rate for heat sink/source outlet temperature

Fig. A.6 PI control system